Investigating the Structural and Functional Roles of Conserved Cysteine Residues in *Arabidopsis thaliana* Fatty-Acid Desaturase 2

By

Lauren Novotny

December 2022

Director of Thesis: Beth Thompson

Major Department: Biology

Abstract

Plant-generated unsaturated fatty acids (UFAs) and polyunsaturated fatty acids (PUFAs) are vital to a plant's growth and survival through maintenance of plasma membrane fluidity and integrity, in addition to the various functions lipids carry out within all organisms. These compounds are also in high demand due to human reliance on their incorporation into everyday diets, products, and the increasing field of research into biofuels. Fatty acid desaturases (FADs) are key enzymes in the synthesis of these biomolecules, but limited research into the diverse subgroup of membrane-bound desaturases has been performed. Plant fatty acid desaturase 2 (FAD2) is a microsomal enzyme that introduces a carbon-carbon double bond at the Δ12 position of oleic acid through an oxygenated intermediate to form linoleic acid, and as a membrane-bound desaturase it remains structurally uncharacterized. Sequence comparison of FAD2 from model organism *Arabidopsis thaliana* to plant species expressing homologous proteins has uncovered seven cysteines conserved to various degrees that we hypothesized to play distinct roles in the structure and function of FAD2. To evaluate this concept, site-directed mutagenesis of each cysteine to alanine was performed followed by transient expression of FAD2 in *Saccharomyces cerevisiae.* Preliminary lipid compositional analysis by gas chromatography has demonstrated that each cysteine mutation resulted in reduced enzymatic

activity with two mutations completely depleting activity. These results brought into question the involvement of each cysteine in the established homodimer protein-protein interaction and overall protein stability. By determining the roles of the conserved cysteines within FAD2, more will be understood about the enzyme structure and mechanism which can be applied to other similarly uncharacterized membrane-bound FADs in plant systems. Ultimately, a better understanding of these enzymes will inform rational engineering strategies for producing essential lipids and high value bioproducts.

Investigating the Structural and Functional Roles of Conserved Cysteine Residues in *Arabidopsis thaliana* Fatty-Acid Desaturase 2

A Thesis

Presented To the Faculty of the Biology Department

East Carolina University

In Partial Fulfillment of the Requirements for the Degree

M.S., Molecular Biology and Biotechnology

by

Lauren Novotny

December, 2022

Director of Thesis: Beth Thompson, PhD

Thesis Committee Members:

Patrick J. Horn, PhD

Adam Offenbacher, PhD

Eric Anderson, PhD

Investigating the Structural and Functional Roles of Conserved Cysteine Residues in *Arabidopsis thaliana* Fatty-Acid Desaturase 2

By

Lauren Novotny

APPROVED BY:

Director of Thesis _____
Beth Thompson, PhD

Committee Member _____
Patrick J. Horn, PhD

Committee Member _____
Adam Offenbacher, PhD

Committee Member _____
Eric Anderson, PhD

Chair of the Department of Biology _____
David Chalcraft, PhD

Interim Dean of the Graduate School _____
Kathleen Cox, PhD

TABLE OF CONTENTS

LIST OF FIGURES

LIST OF ABBREVIATIONS

CHAPTER 1: INTRODUCTION

1.1 Lipids and Fatty Acid Desaturases (FADs)

Lipids are one of the four groups of macromolecules required in all organisms to carry out various functions including but not limited to signaling, structure, energy storage, and membrane composition (Muro et al. 2014). Within plants, these molecules are critical for growth and survival as they maintain plasma membrane fluidity and integrity, which in turn allows the plant to tolerate environmental stressors such as extreme temperature fluctuation and salinity (Halim et al. 2022). To accomplish this, plants produce a wide variety of fatty acids, many of which mammals are either unable to make at all or unable to make without the dietary input of their ω3 and ω6 fatty acid precursors (Simopoulos 2010; Simopoulos 2016). Due to this inability in mammals, these compounds are instead incorporated through diet since low levels in humans have been found to be correlated with alarming health issues such as cardiovascular diseases, poor fetal development, Alzheimer's disease, bipolar affective disorders, schizophrenia, and further inflammatory conditions (Halim et al. 2022). In addition to being a dietary requirement, plant lipids are also incorporated into products like cosmetics, surfactants, lubricants, paints, and plastics which has created an increasing demand for high-yield oil crops that produce desaturated fatty acids (Murphy 2016; Ahmad & Ahsan 2020; Biermann et al. 2021). This increased demand has only intensified in recent years as research into "green" alternatives to fossil fuels has grown (Ambaye et al. 2021). But the limiting factor of production and progress in these areas is the fact that high-yield oil crops are only currently capable of producing a limited variety and quantity of desirable fatty acids- an issue that metabolic engineering of FADs aims to overcome in the future.

FADs are a family of enzymes that catalyze the removal of two hydrogens from fatty acids using a reactive oxygen intermediate to establish carbon-carbon double bonds and generate unsaturated fatty acids (UFAs) and polyunsaturated fatty acids (PUFAs) (Cahoon & Shanklin 2000). The synthesis of these substrate molecules in plants primarily occurs in the plastid where 16- or 18-carbon chains are generated from small precursors (Ohlrogge & Browse 1995) and in this stage are categorized as saturated fatty acids. It is in this organelle where the first and most abundant class of FAD is encountered- soluble desaturases. These desaturases are biochemically and structurally well characterized due to their abundance and ability to be studied with *in vitro* methods and have therefore contributed to the majority of compiled information on FADs (Lou et al. 2014; Halim et al. 2022). But as soluble desaturases are mostly just responsible for the desaturation of stearoyl-ACP (18:0-ACP) to oleoyl-ACP (18:1-ACP) (Nachtschatt et al. 2020), the second class of FADs- integral membrane/membrane-bound desaturases- is of particular interest to high-yield oil crop bioengineers due to their production of a wide array of PUFAs.

Membrane-bound desaturases, opposed to the soluble desaturases, have been found in a wide variety of subcellular locations and differ in sequence, function, and substrates (Shanklin & Cahoon 1998). Analysis of sequence similarity and regiospecificity has led to the discovery of four distinct groupings- front-end desaturases, first desaturases, methyl-end desaturases, and Δ4 sphingolipid desaturases. Front-end desaturases are classified as those that introduce the carbon-carbon double bond near the carboxyl end of the lipid, first desaturases introduce the double bond at the Δ9 position, methyl-end desaturases introduce the double bond near the methyl end of the lipid, and Δ4 sphingolipid desaturases act on the Δ4 position (Li et al. 2016). Although these substrates displaying enzyme specificity have been identified, further details on substrate recognition and mechanism of action remain unclear and are truly puzzling as the ability of an

enzyme to distinguish between essentially equivalent long-chain fatty acids seems improbable (Chen et al. 2013). This lack of understanding stems from the fact that membrane-bound desaturases are poorly characterized in terms of structure (Lou & Shanklin 2010) due to insufficient amounts of protein and difficulty in purifying the proteins in their native forms. Despite these obstacles, crystal structures of two integral membrane desaturases have been experimentally determined- PDB: 4ZR1 (a yeast sphingolipid α-hydoxylase) and 4ZYO (a mammalian Δ9 desaturase). Sequence comparisons of many members of the membrane-bound desaturase family to these two proteins indicates that common features may include a "mushroom-like" structure where the N- and C-terminal ends exist in a catalytic cap domain situated on the cytosolic face, hydrophobic helices span the membrane, and conserved histidine boxes that bind two iron ions make up the active site (Nachtschatt et al. 2020). But even with these findings, many differences exist between the wide variety of integral membrane desaturases and will therefore need to be assessed on an individual basis.

1.2 Fatty Acid Desaturase 2 (FAD2)

FAD2 from *Arabidopsis thaliana* is an endoplasmic reticulum transmembrane protein classified as a methyl-end desaturase (Lee et al. 2016). FAD2 specifically acts on oleic acid (18:1Δ^{9}-phosphatidylcholine, PC) to form linoleic acid (18:2$\Delta^{9,12}$-PC; Fig. 1) in plants. It may also catalyze the conversion of palmitoleic acid (16:1Δ^{9}-PC) to form hexadecadienoic acid (16:2$\Delta^{9,12}$-PC; Liu et al.

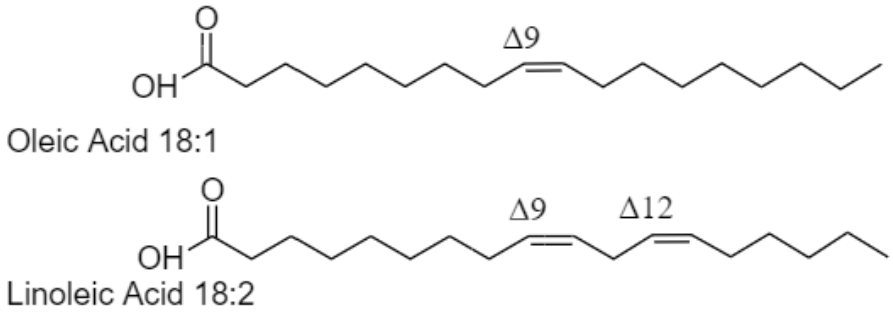

Figure 1. Fatty acid structures of FAD2 substrate, oleic acid, and resulting PUFA, linoleic acid.

2019), although the latter reaction is primarily observed in *Saccharomyces cerevisiae* upon heterologous expression. Apart from PUFA synthesis, FAD2 has also been linked to functions such as salt tolerance during seed germination, early seedling growth, and vegetative growth (Ben Ayed et al. 2022). This is due to the fact that endoplasmic reticulum membrane lipid polyunsaturation is mediated by FAD2 in *Arabidopsis* (Nguyen et al. 2019), and this desaturation is required to maintain proper function of Na^+/H^+ channels to keep cytosolic Na^+ concentrations low to aid in cellular salt tolerance (Zhang et al. 2012). Pairing these functions with the fact that linoleic acid is the PUFA that is most heavily incorporated into human diets (Whelan & Fritsche 2013), it is evident that FAD2 is an important enzyme to study further.

Similar to other plant integral membrane-bound FADs, the structure of FAD2 has yet to be experimentally determined. Despite this, sequence analysis has identified characteristic conserved regions that could indicate structural and/or functional domains. These include two long stretches of hydrophobic amino acids and three histidine-rich boxes, which, when incorporated into a topological model suggests that the enzyme could be anchored into the endoplasmic reticulum by four membrane-spanning regions with the histidine boxes, N- and C-termini all facing the cytosolic side of the membrane (Dyer & Mullen 2001) (Fig. 2). Experiments using fusion tags to the N- and C-termini performed by Dyer and Mullen confirmed their location relative to the membrane. All of the previously mentioned features are typical of FADs which therefore suggests the histidine boxes are the active site of FAD2 as

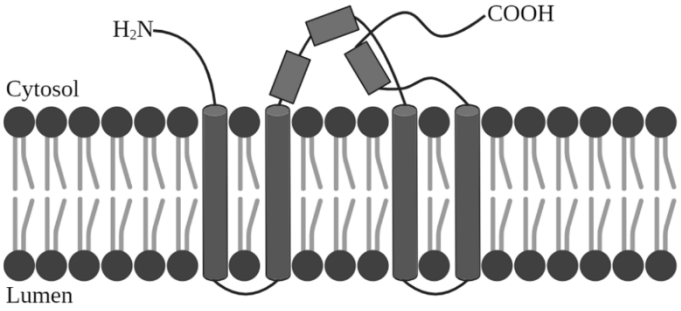

Figure 2. Topology diagram of FAD2 as proposed by Dyer & Mullen 2001 displaying regions conserved within FADs. Histidine boxes are represented as rectangles. Created with BioRender.com.

well. Further efforts to uncover the structure of FAD2 have utilized the previously mentioned crystal structure of human stearoyl-CoA desaturase (HsSCD) (Wang et al. 2015) to generate a homology model (Fig. 3). This was done by using the HsSCD crystal structure as a template over

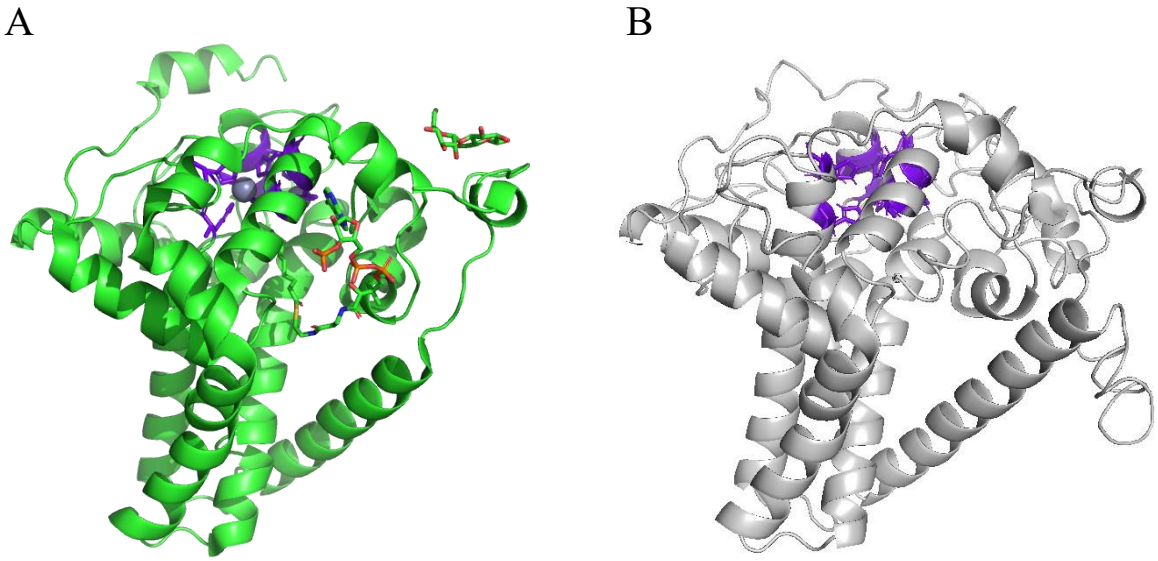

Figure 3. A. Crystal structure of human stearoyl-CoA desaturase (PDB ID: 4ZYO) with two zinc ions coordinated in conserved histidine box active site (purple), dodecyl-beta-d-maltoside interacting at the top right, and stearoyl-coenzyme A interacting in the middle. B. Homology model of FAD2 generated by PI Horn with I-TASSER using HsSCD as a template, refined using ModRefiner, and checked with ProCheck. Conserved histidine box is shown in purple.

which the sequence of FAD2 was "threaded" upon identification of sequence similarities through sequence alignment, and optimized based on knowledge-based energy function, spatial constraints, and accepted folding properties (Sliwoski et al. 2014). However, sequence deviations, substrate preferences, and different parent organisms are likely to contribute to decreased confidence within certain regions, and therefore highlights limitations of the model. In addition, FAD2 has been found to form a heterodimer with fatty acid desaturase 3 (FAD3) and a homodimer with itself both in *Arabidopsis* and when expressed in *Saccharomyces cerevisiae* (Lou et al. 2014). The previously mentioned structurally characterized proteins have not been reported to be involved in comparable homodimer or heterodimer interactions, so therefore despite software generated protein-protein docking models (Fig. 4), questions remain about the

conformation, orientation, and purpose of dimers. To gain further insight into uncharacterized aspects such as the functional mechanism, nature of interactions with proteins, and predicted responses to environmental or chemical changes, the structure of FAD2 needs to be experimentally evaluated.

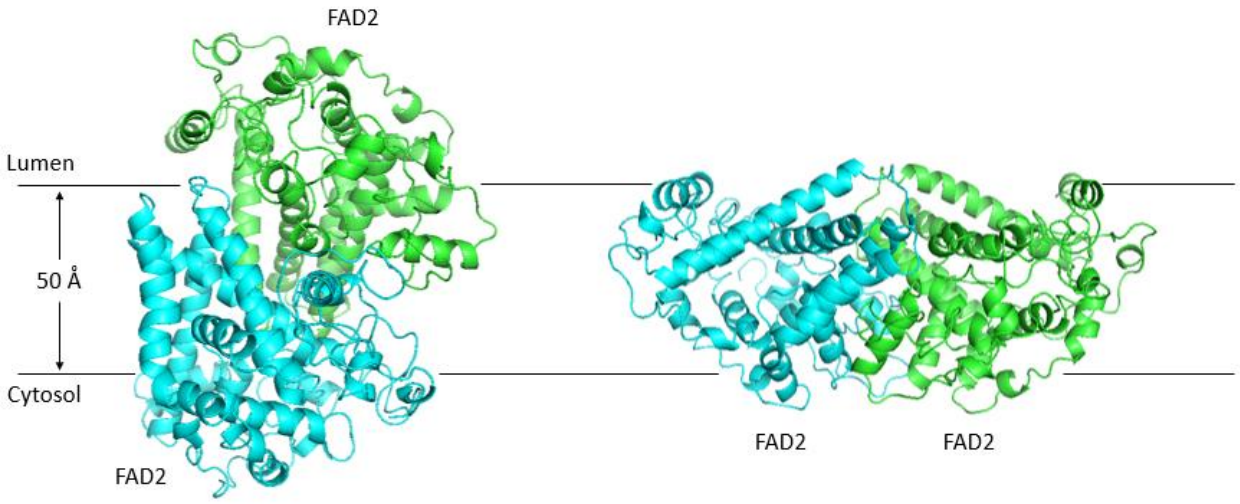

Figure 4. Potential homodimerization of FAD2 in the ER membrane generated via ClusPro.

1.3 Cysteine in Proteins

As conventional methods (such as X-ray crystallography or nuclear magnetic resonance) of experimentally determining the structure of FAD2 have been unsuccessful thus far, alternative methods such as analyzing specific amino acids within the protein sequence to determine their role can be employed. An amino acid that is known to play various roles within proteins is cysteine- a polar, noncharged (at physiological pH) residue that is one of the least abundant amino acids found in nature (Marino & Gladyshev 2012). Despite this, cysteine is overrepresented in functional sites of proteins to be involved in activities such as cofactor-binding, catalysis, and regulatory functions as a result of being highly reactive, polarizable, redox-active, and containing a high-affinity for metals (Burns et al. 2016; Marino & Gladyshev 2010). In catalysis, two cysteines are usually involved, where one initiates a nucleophilic attack on the substrate, after which the second attacks the enzyme-substrate intermediate (Marino et al.

2022). Cysteines can also serve regulatory functions as a result of posttranslational modifications including S-nitrosylation, sulfhydration, S-glutathionylation, disulfide bonds, sulfenylation, sulfinic acid, and sulfonic acid (Chung et al. 2013) which can alter protein conformation, localization, interactions, and activity (Bassot et al. 2021). Coordination of metals like zinc, copper, and iron can aid in stabilizing protein structure as well as providing an important component for active-site chemistry (Marino & Gladyshev 2010). A further contribution of cysteines to the structure of proteins is disulfide bonds, which will stabilize the protein and influence tertiary and/or quaternary structure (Fra et al. 2017) if the thiol groups are within 2.05-3.0Å and have a pK_a~8.5 (Sun et al. 2017).

Among a variety of plant species with homologous proteins to FAD2, seven cysteines have been found to be conserved to various degrees within the protein sequence (Fig. 5). This

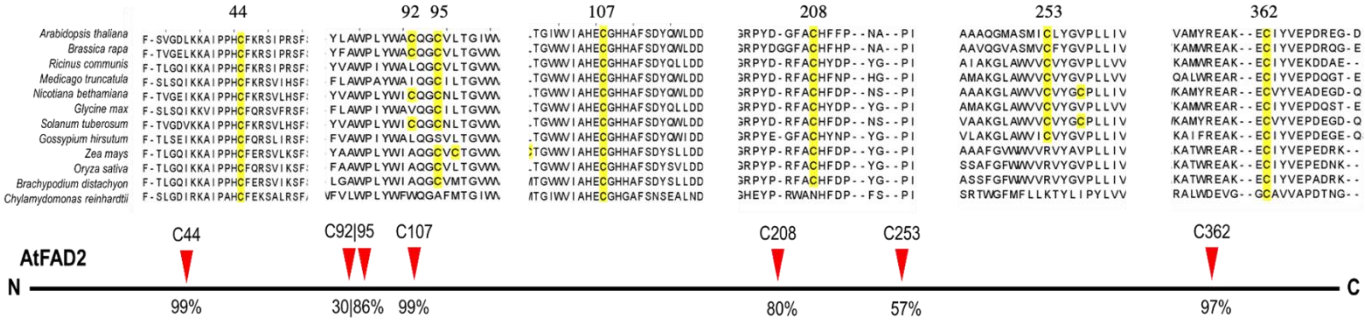

Figure 5. Representative global sequence alignment illustrating cysteine conservation in ten different plant species courtesy of Parth Dave.

conservation likely indicates the importance of these cysteines for protein function (in enzymatic, structural, or regulatory roles) as cysteines appear to be under strict evolutionary control (Marino & Gladyshev 2010). Visualization of the conserved cysteines on the proposed homology model (Fig. 6) suggests that they are widely distributed throughout the protein structure and could therefore fulfill a variety of the previously mentioned roles. Four of the cysteines (Cys44, 95, 208, and 362) appear to be on the periphery of the protein and could

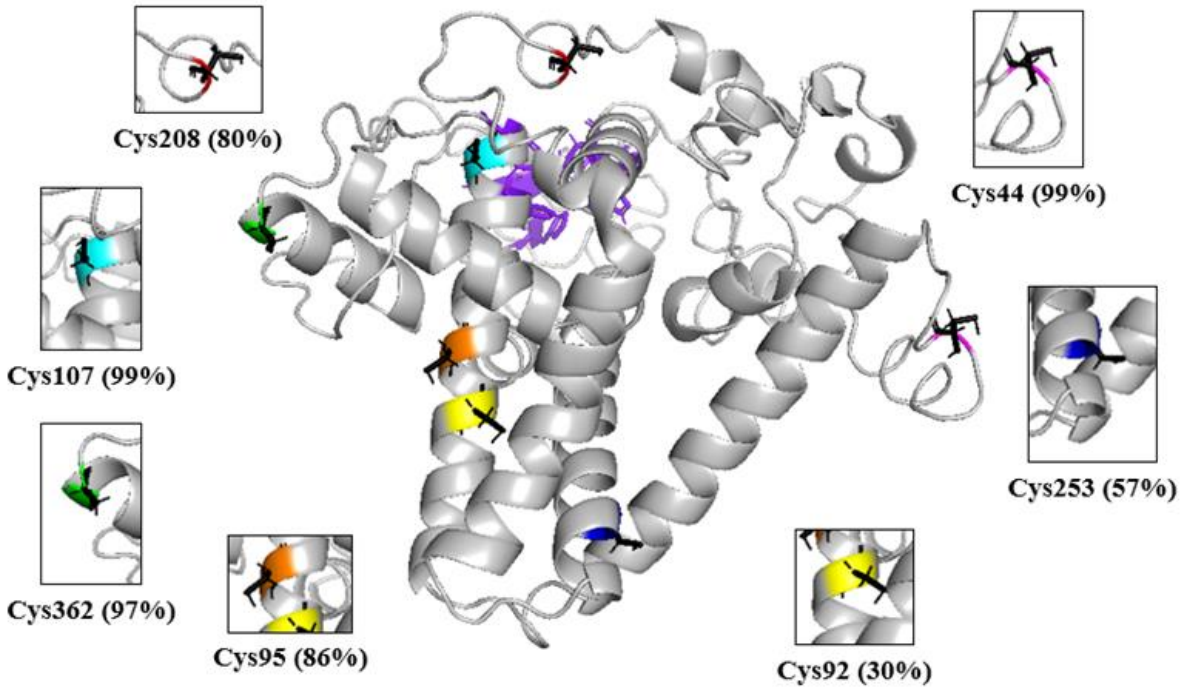

Figure 6. Conserved cysteines within FAD2. FAD2 homology model was generated by PI Horn with I-TASSER using HsSCD as a template, refined using ModRefiner, and checked with ProCheck. Percentages indicate degree of conservation determined from global sequence alignments of FAD2 homologs from 132 plant species genomes. Conserved histidine box is shown in purple.

therefore be involved in protein-protein interactions (PPIs). More interior cysteines (like Cys92, 107, and 253) may not be directly involved in protein-protein interactions but could contribute to structure and stability overall or in interacting regions. Cys92 and 95 are part of a putative CXXC motif and thus may be involved in metal coordination or as a redox-active switch (Gladyshev et al. 2004) that is found to be conserved outside the predicted catalytic site of nearly all fatty acid desaturase 4 (FAD4) eudicot sequences (Horn et al. 2020). Additionally, due to their perceived proximity, a disulfide bond may exist between Cys92 and 95 to contribute to protein stability. Finally, Cys107 and 208 may be important to the FAD2 activity of desaturation as they are predicted to be close to the conserved histidine box active site.

One approach to elucidate the function of these conserved cysteines in FAD2 is to individually mutate each to alanine (Fig. 7). Alanine is a non-polar, hydrophobic amino acid that

is non-reactive and therefore rarely involved in protein function (Betts & Russell 2003). By substituting each cysteine for alanine, any conserved structural or functional roles should be diminished, allowing further experimentation and analysis to uncover that role. Similar approaches have used serine instead of alanine due to its favorability as a substitution for cysteine in membrane proteins (Betts & Russell 2003), but because of its fairly reactive hydroxyl group, it was not used in an attempt to prevent hydrogen bonding and potential redox activity as part of a CXXS motif (Fomenko & Gladyshev 2002). Preliminary experiments performed by PI Horn and former undergraduate student Parth Dave utilized this concept to assess the role of each cysteine in the biosynthetic function of FAD2. Lipid profile analysis was performed using *S. cerevisiae* expressing the cysteine-to-alanine mutant proteins (generated through primer-based site-directed mutagenesis (SDM) of the FAD2 coding sequence) from pESC-HIS plasmids (Agilent Technologies) in comparison to the wild-type protein (Fig. 8). The results of this experiment indicated that there is a decrease in FAD2 activity for many of the mutated proteins (mainly FAD2-C107A, C208A, and C362A). This preliminary finding highlights the need for further investigation as FAD2 activity would have remained the same if the mutated cysteines did not play a significant role within FAD2.

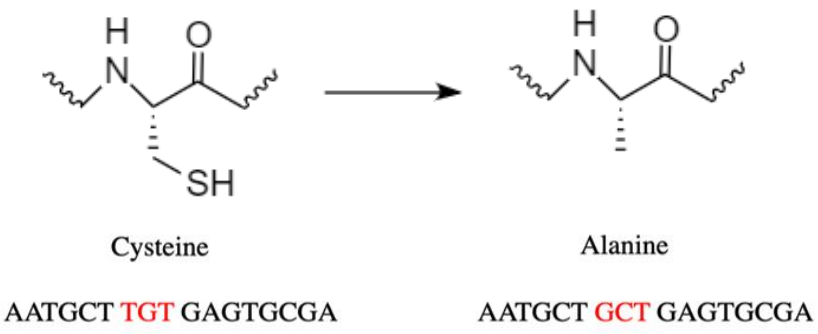

Figure 7. Illustration of cysteine to alanine mutation displaying the amino acids structures as they exist in proteins and their corresponding codon labeled in red.

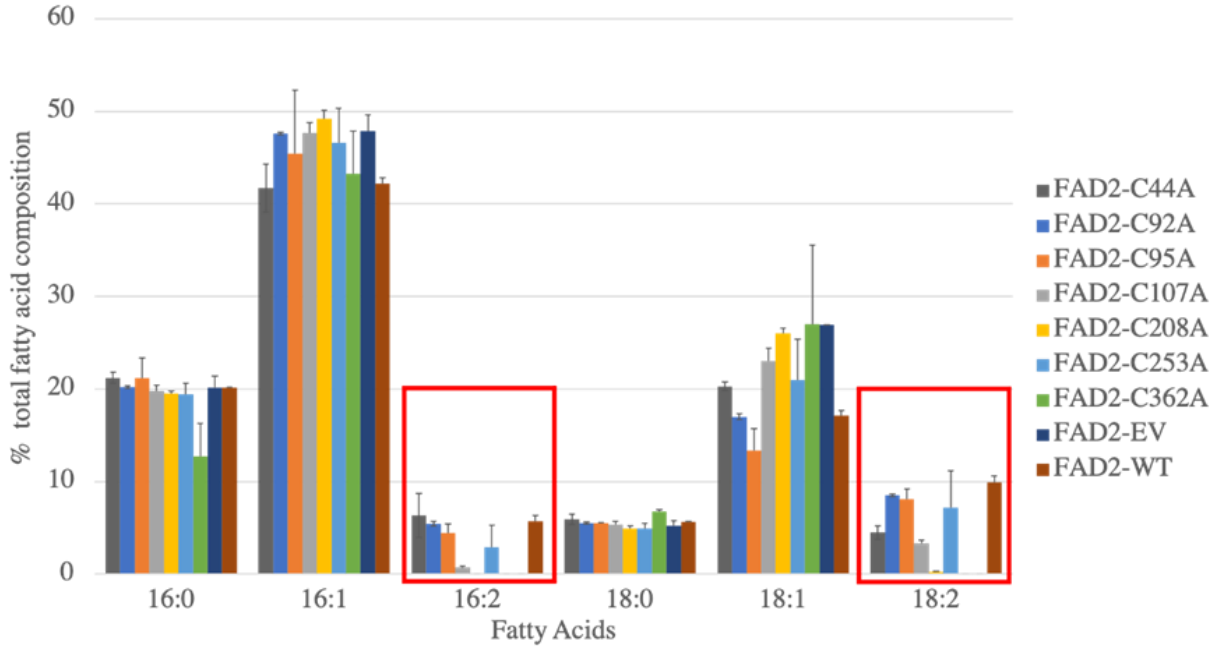

Figure 8. Percent total fatty acid composition as a result of FAD2 cysteine-to-alanine mutations in yeast (courtesy of Parth Dave). Red boxes indicate fatty acids produced by FAD2.

1.4 Summary of Thesis Aims

FADs are vital to the production of UFAs and PUFAs that are in high demand due to their incorporation into diets, everyday products, and "green" biofuels, and therefore gaining an increased understanding of this group of enzymes could inform bioengineering efforts to generate proteins with improved stability and/or activity. Despite soluble FADs being highly characterized, little is known about the more diverse class of membrane-bound desaturases due to difficulties encountered in experimentally determining their structures. FAD2 from *Arabidopsis* is not an exception to this trend but has yet to be analyzed further with alternative biochemical methods aimed at uncovering the structural and functional roles of conserved cysteine residues. I set out to begin this type of analysis with the following aims:

1. Detect FAD2 homodimer protein-protein interactions (PPIs) as a result of site-directed cysteine mutations in *S. cerevisiae*.
2. Assess protein formation/stability as a result of cysteine mutations in *S. cerevisiae*.

3. Confirm preliminary data indicating that the cysteine mutations decreased FAD2 function in *S. cerevisiae*.

CHAPTER 2: MATERIALS AND METHODS

2.1 Generating FAD2 Site-Directed Mutants

The coding sequence of the protein of interest, FAD2 (*AT3G12120*), was previously cloned into the yeast episomal plasmid, pESC-HIS (Agilent Technologies), using the EcoRI restriction site which resulted in the addition of a C-terminal FLAG epitope tag. This plasmid was then used along with the Q5® Site-Directed Mutagenesis Kit (New England BioLabs) to generate seven different FAD2 mutants. Custom forward and reverse primers were designed to individually mutate each conserved cysteine to alanine by replacing the cysteine codon (TGT) with alanine (GCT) (Appendix A). The mutations were introduced by the primers during PCR, after which the remaining steps of the Q5® Site-Directed Mutagenesis Kit protocol were followed, culminating in the transformation of each mutated plasmid into NEB 5-alpha competent *E. coli* cells. To verify successful mutagenesis, the plasmid DNA was purified from the transformed cultures using the Monarch® Plasmid Miniprep Kit (New England BioLabs) and analyzed by Sanger sequencing (Retrogen Inc.). Upon confirmation of the desired sequences, the plasmids were then transformed into competent *S. cerevisiae* cells, strain INVSc1 (Mata his3D1 leu2 trp1-289 ura3-52), using the Frozen-EZ Yeast Transformation II Kit™ (Zymo Research).

2.2 Cloning FAD2 for mbSUS

The purified pESC-HIS plasmids containing wild-type or mutant FAD2 coding sequences were used further as template DNA in PCR to amplify the coding sequences with the addition of B1 and B2 linker sites through use of custom primers (Appendix A). Amplified products were run on a 1% (w/v) agarose gel via electrophoresis, excised, and then purified using the Wizard® SV Gel and PCR Clean-Up System (Promega). Plasmids to be used in the mbSUS system, pNXgate32-3HA (containing a N-terminal ubiquitin fusion, or Nub) and pMetYCgate

(containing a C-terminal ubiquitin fusion, or Cub; Addgene), were digested (pNXgate32-3HA with SmaI for one hour at 25˚C then with EcoRI for one hour at 37˚C; pMetYCgate with PstI and HindIII for one hour at 37˚C), run on a 1% (w/v) agarose gel, excised, and purified with the Wizard® SV Gel and PCR Clean-Up System. Transformation reactions were set up with boiled carrier-salmon sperm DNA (5 mg/mL), linearized plasmid (100 ng), purified insert (>100 ng), 1 M LiAc, competent cells (THY.AP5 [Mat α] for pNXgate32-3HA transformations, THY.AP4 [Mat a] for pMetYCgate transformations), and a 50% PEG/1 M LiAc mix. Reactions were incubated with shaking for 20 minutes at 30˚C, followed by a heat-shock for 20 minutes in a 42˚C water bath, then centrifugation at 6000-8000 rpm for one minute. Pellets were resuspended in sterile ddH_2O before being streaked on appropriate selection media (SC-Trp for THY.AP5 [Mat α] containing pNXgate32-3HA; SC-Leu for THY.AP4 [Mat a] containing pMetYCgate) which was grown for 2-4 days at 30˚C.

2.3 Analyzing FAD2 PPIs in the Mating-Based Split Ubiquitin System (mbSUS)

To detect FAD2 protein-protein interactions in yeast, a modified version of the mating-based split ubiquitin system (Obrdlik, 2004) was implemented. The previously transformed haploid strains (THY.AP5 [Mat α] and THY.AP4 [Mat a]) were allowed to mate for five hours in YPAD media (0.0075% (w/v) 1-adenine hemisulfate salt, 1% (w/v) yeast extract, 2% (w/v) Bacto peptone, 2% (w/v) dextrose) with shaking at 200 rpm at 30˚C for each combination to be tested (mutant-Nub with mutant-Cub, mutant-Nub with wild-type-Cub, wild-type-Nub with mutant-Cub, as well as controls). Dilutions of each culture in ddH_2O were then made to concentrations of 1 (undiluted), 0.1, 0.01, and 0.001 in a 96-well plate. These dilutions were then spot plated on SD+Ade+His (0.67% (w/v) yeast nitrogen base without amino acids, 2% (w/v) Bacto agar, 2% (w/v) dextrose, 0.002% (w/v) Histidine, 0.004% (w/v) Adenine) and SC-Ade-

His-Leu-Trp-Ura-Met (Drop-out Mix Minus Adenine, Histidine, Leucine, Methionine, Tryptophan, Uracil w/o Yeast Nitrogen Base Powder and Drop-out Base (w/o aa) With Glucose and Agar Powder, USBiological Life Sciences) plates and allowed to dry before incubation for two days and four days, respectively, at 30˚C. After two days, the SD+Ade+His plates were imaged before proceeding to the X-Gal assay to detect β-galactosidase expression and activity as a result of PPIs. The X-Gal assay began with flooding the plates with chloroform for five minutes to permeabilize the cells, after which the chloroform was decanted off and the plates were inverted on a rack for another five minutes to dry. Plates were then overlayed with Z-buffer (10.68 g/L $Na_2HPO_4 \times 2H_2O$, 5.5 g/L $NaH_2PO_4 \times H_2O$, 0.75 g/L KCl, 0.246 g/L $MgSO_4 \times 7H_2O$) with added 10% (w/v) sodium dodecyl sulfate (SDS), 2 mg/mL X-Gal in dimethylformamide, and 0.005 g/mL agarose before being incubated for 24 hours at 30˚C. The assay concluded with imaging the plates to visualize results, with blue colonies indicating a PPI occurred, and white colonies indicating no PPI. The SC-Ade-His-Leu-Trp-Ura-Met plates were imaged after four days, with colony growth indicating PPI, and no growth indicating no PPI.

2.4 Cloning FAD2 for Protein Analysis

The pESC-HIS plasmid containing wild-type FAD2 was again used as template DNA in PCR to amplify the coding sequence and add XhoI restriction sites to both ends of the sequence. Amplified products were run on a 1% (w/v) agarose gel via electrophoresis, excised, and then purified using the Wizard® SV Gel and PCR Clean-Up System. This purified product was then digested with XhoI for one hour at 37˚C before once again being cleaned up by the Wizard® SV Gel and PCR Clean-Up System. The episomal plasmid, pESC-LEU (Agilent Technologies), was then digested with XhoI for two hours at 37˚C, run on a 1% (w/v) agarose gel, excised, and purified with the Wizard® SV Gel and PCR Clean-Up System. The 5’ ends of the cut plasmid

were then dephosphorylated using the Quick Dephosphorylation Kit (New England BioLabs), and the heat-inactivated solution was cleaned up with the Wizard® SV Gel and PCR Clean-Up System. A ligation reaction using T4 DNA Ligase (New England BioLabs) was then performed overnight at 16˚C with the XhoI digested FAD2 DNA insert and the cut pESC-LEU plasmid in an 8:1 molar ratio. The ligated product was then transformed into TOP10F $CaCl_2$ *E. coli* cells through a 45 second heat shock at 42˚C followed by an hour incubation at 37˚C with 200 rpm shaking in SOC media (2% (w/v) Bacto-tryptone, 0.5% (w/v) yeast extract, 10 mM NaCl, 2.5 mM KCl, 10 mM $MgCl_2 \times 6H_2O$, 10 mM $MgSO_4 \times 7H_2O$, 20 mM glucose). The transformation was then plated on LB+Amp (100 μg/mL ampicillin) plates and incubated overnight at 37˚C. To verify successful ligation and transformation, colony PCR with insert-specific primers was performed followed by visualization on a 1% (w/v) agarose gel. Upon verification, plasmids purified from successfully transformed colonies were transformed into competent *S. cerevisiae* cells, strain INVSc1, using the Frozen-EZ Yeast Transformation II Kit™. Due to time constraints and a low rate of success, the pESC-LEU plasmid containing wild-type FAD2 was then used along with the Q5® Site-Directed Mutagenesis Kit and custom primers to generate the cysteine 107 to alanine mutation using the same protocol as previously mentioned. The two generated pESC-LEU-myc-FAD2 plasmids were sequenced, and the mutated plasmid was transformed into competent *S. cerevisiae* cells, strain INVSc1, using the Frozen-EZ Yeast Transformation II Kit™.

2.5 Yeast Protein Expression Time Course

To obtain samples of the wild-type and cysteine-to-alanine mutated FAD2 proteins for stability analysis, a protein expression time course was performed using the previously mentioned pESC-LEU plasmids. Cultures were started from one colony that was inoculated into

SD-LEU media (0.67% (w/v) yeast nitrogen base without amino acids, 2% (w/v) dextrose, 0.07% (w/v) -LEU dropout supplement Clontech Cat #630416) and incubated overnight at 30˚C with 300 rpm shaking. Total OD600 absorbance of each overnight culture was measured via spectrophotometer before being pelleted down and resuspended in SGal-LEU (0.67% (w/v) yeast nitrogen base without amino acids, 2% (w/v) galactose, 0.07% (w/v) -LEU dropout supplement Clontech Cat #630416) induction media at 0.4 OD. Inducted cultures were grown to mid-log phase (~1.0 OD) at 22˚C with 300 rpm shaking before treatment was added (dimethylsulfoxide (DMSO) as a control or 0.5 mg/mL cycloheximide to stop translation) to begin the time course. Aliquots of 2.0 OD were taken from each culture at 0, 1-, 2-, 4- and 8-hours post-treatment for protein analysis and 10.0 OD aliquots were taken at hour zero for lipid profile analysis.

2.6 Protein Extraction, SDS-PAGE, and Western Blot Analysis

Total protein was extracted from the saved 2.0 OD aliquots previously mentioned starting with a five-minute incubation at room temperature in 200 mM NaOH. Samples were then pelleted at 1500xg for five minutes, the supernatant was removed, and pellets were resuspended in 1X SDS sample buffer (63 mM Tris-HCl pH 6.8, 10% (v/v) glycerol, 2% (w/v) SDS, 0.01% (w/v) bromophenol blue, 5% (w/v) beta-mercaptoethanol, 16.7% (v/v) protease cocktail inhibitor (Roche), 53.3% ddH_2O) before being boiled for 5-10 minutes in a dry heater at 95˚C. Samples were once again pelleted at maximum speed for three minutes, and the resulting supernatant was loaded onto Mini-PROTEAN TGX Stain-Free Gels (BioRad) for SDS-PAGE.

Prior to loading the gels, the gel box was filled with 1X SDS-PAGE Running Buffer (30 g/L Tris Base, 144 g/L glycine, 10 g/L SDS, pH 8.3), and a standard ladder (Pierce™ Prestained Protein MW Marker) was loaded alongside the samples. Gels were run at 50 V for ~15 minutes

before the voltage was increased to 100 V for an hour or until the loading dye reached the bottom of the gel. The gels were then removed and imaged on a ChemiDoc (BioRad).

A Trans-Blot Turnbo Transfer System (BioRad) was then used to transfer proteins from the gel to a PVDF membrane using the Mixed MW protocol. This membrane was then washed with 1X Tris-Buffered Saline (TBS) (200 mM Tris Base, 1.5 M NaCl) with shaking at room temperature for five minutes. Blocking was then performed for one hour at room temperature using blocking buffer (5% (w/v) nonfat dry milk in TBS with Tween20 (TBST)), after which it was washed three times for five minutes each with TBST. The membrane was then incubated overnight at 4˚C with the primary antibody (Anti-Myc Tag Antibody, clone 9E10 from mouse (Millipore Sigma)) in dilution buffer (5% (w/v) nonfat dry milk in TBST), followed by another three washes for five minutes each with TBST. The secondary antibody (Goat anti-Mouse IgG (H+L)-HRP Conjugate (BioRad)) in dilution buffer was then added at room temperature for one hour before the membrane was washed a final three times in TBST. The Clarity Western ECL Substrate Kit (BioRad) was used to aid in detection, and the membrane was imaged on the ChemiDoc.

The same membrane was then stripped using harsh stripping buffer (10% (w/v) SDS, 0.5 M Tris HCl pH 6.8, 0.8% (w/v) beta-mercaptoethanol, heated to 50˚C) for 45 minutes at 50˚C with agitation. Running tap water was used to rinse the stripped membrane for 1-2 minutes, followed by three extensive washes for five minutes in TBST. The same protocol as detailed above was then implemented (starting with blocking for one hour) with the only modification being the primary antibody- monoclonal anti-DPM1 (dolichol phosphate mannose synthase) antibody produced in mouse (Invitrogen) was used to detect the loading control. Image Lab software (BioRad) was used to perform densitometric analysis of corresponding blots.

2.7 Gas Chromatography Analysis

Lipids were extracted from the saved 10.0 OD aliquots previously mentioned through an acid-catalyzed direct transmethylation method. Each sample (pelleted with water removed) was treated with 1 N methanolic HCl, toluene, and 1 mg/mL 15:0 FFA standard before being vortexed for 30 seconds and heated at 80˚C for 30 minutes. The samples were allowed to come to room temperature, then hexane and 1% NaCl were added, the solutions were vortexed for 10 seconds, and then centrifuged at 1500 rpm for three minutes. Hexane from each sample (the upper phase) was then transferred to glass culture tubes and dried using N_2 gas and a 40˚C heater (Organomation Multivap Nitrogen Evaporator). Samples were then resuspended with hexane and transferred to gas chromatography vials. An Agilent 7890 flame ionization detection gas chromatograph with an Agilent J&W DB-23 column was used to analyze and quantify the samples by heating them to 250˚C under 8.6686 psi with total airflow of 11.302 mL/min, column flow of 1.3836 mL/min, average velocity of 40.007 cm/sec, and a septum purge flow of 3 mL/min.

CHAPTER 3: RESULTS AND DISCUSSION

3.1 Cloning of Wild-Type and Mutant FAD2 for Expression in Yeast

To express FAD2 in *S. cerevisiae*, the previously generated pESC-HIS-FAD2-FLAG plasmid was used, and site-directed mutagenesis with custom primers (Appendix A) was employed to introduce individual cysteine to alanine mutations (Fig. 9). Sanger sequencing verified successful mutagenesis and the purified plasmids containing wild-type or mutant FAD2 coding sequences were used to generate plasmids for further experiments. For the mbSUS assay used to assess protein-protein interactions (as discussed in Section 3.2), the coding sequences (CDS) were used as template DNA in PCR before combination with restriction enzyme digested pNXgate32-3HA and pMetYCgate plasmids. The generated plasmids (Fig. 10) were then transformed into *S. cerevisiae* strains THY.AP5 [Mat α] and THY.AP4 [Mat a] cells, respectively. Lastly, to assess FAD2 stability, the wild-type FAD2 CDS from the pESC-HIS

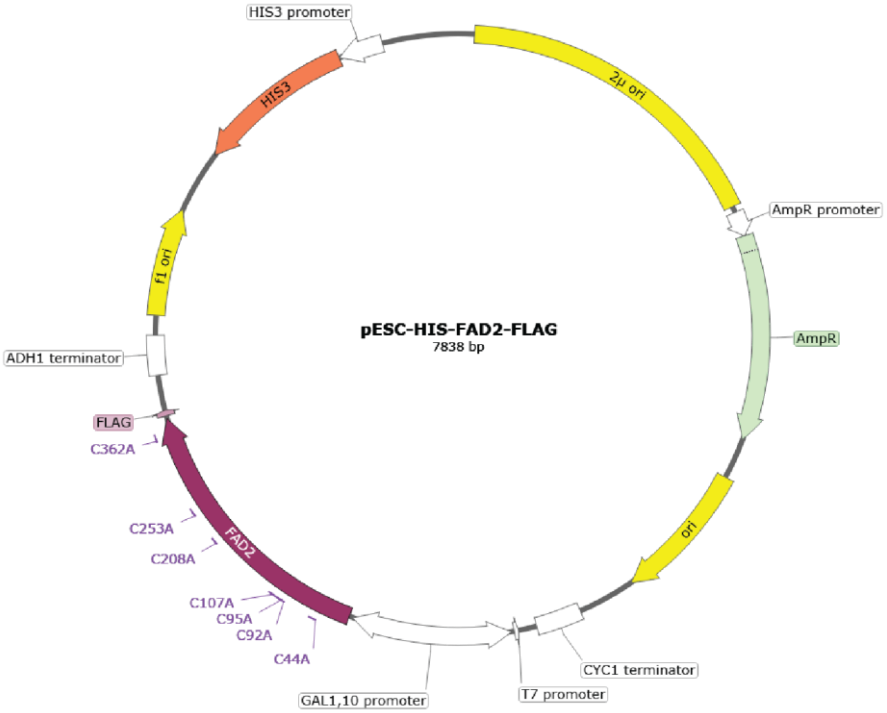

Figure 9. pESC-HIS-FAD2-FLAG plasmid map shown via SnapGene. Arabidopsis *FAD2 CDS is under a GAL1 promoter for galactose-inducced expression, with Cys to Ala mutation locations marked. Noteworthy features include ampicillin resistance, HIS3 for auxotrophic selection in yeast, and a FLAG tag.*

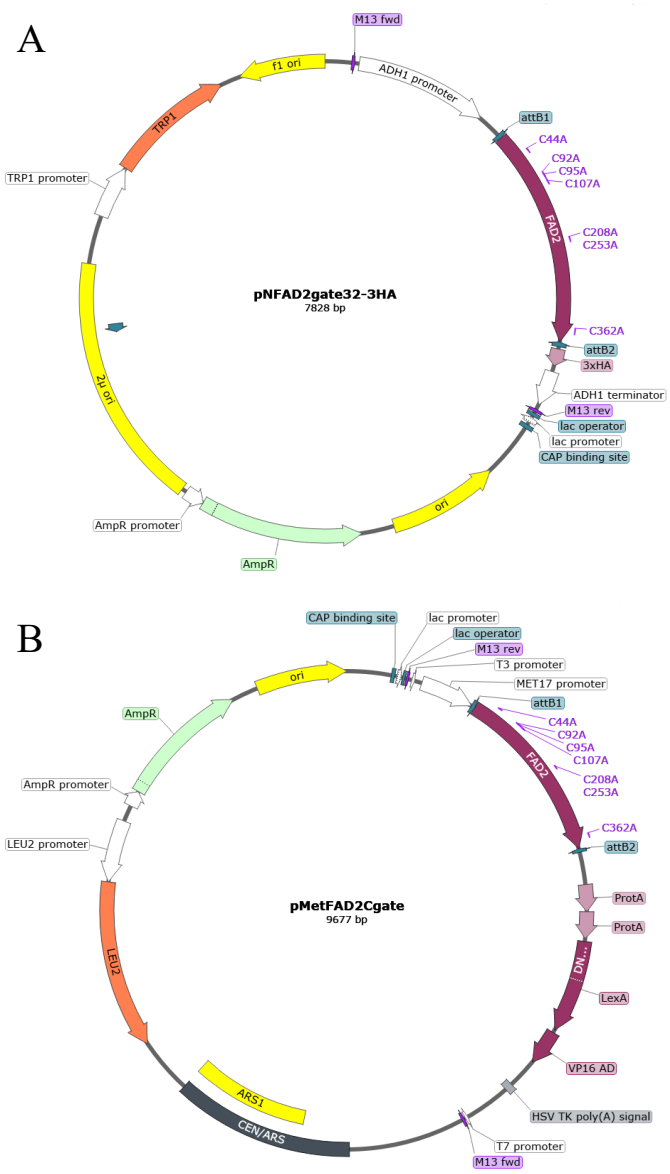

Figure 10. mbSUS plasmid maps shown via SnapGene. A. Bait plasmid (pMetFAD2Cgate) contains Arabidopsis *FAD2 CDS under a MET17 promoter for methionine-controlled expression, with Cys to Ala mutation locations marked. Noteworthy features include ampicillin resistance, LEU2 for auxotrophic selection in yeast, attB1 and attB2 cloning sites, and LexA-VP16 for a reporter molecule. B. Prey plasmid (pNFAD2gate32-3HA) contains* Arabidopsis *FAD2 CDS under a ADH1 promoter, with Cys and Ala mutation locations marked. Noteworthy features include ampicillin resistance, TRP1 for auxotrophic selection in yeast, attB1 and attB2 cloning sites, and a 3xHA tag.*

plasmid was used as template DNA in PCR to add XhoI restriction sites to both ends of the sequence so that the product could be ligated into XhoI digested pESC-LEU (Fig. 11A). Following ligation, the plasmid was transformed into TOP10F $CaCl_2$ *E. coli* cells which was verified through PCR (Fig. 11B), and positive transformants were used to produce higher concentrations of the plasmid for transformation into *S. cerevisiae* strain INVSc1 and site-directed mutagenesis. As a result of minimal success with site-directed mutagenesis, only the C107A mutation was introduced (Fig. 11C) and successfully transformed into yeast (Fig. 11D) for further analysis. Apart from the C253A mutation, the remaining cysteines were not successfully mutated to alanine (as demonstrated by the lack of bands in Fig. 11C) despite multiple attempts of site-directed mutagenesis. The C253A mutation was in fact introduced and

verified through sequencing of the region, but after transformation of the plasmid into yeast, no colonies grew on leucine deficient auxotrophic selection plates, leading to the conclusion that another region of the plasmid was damaged.

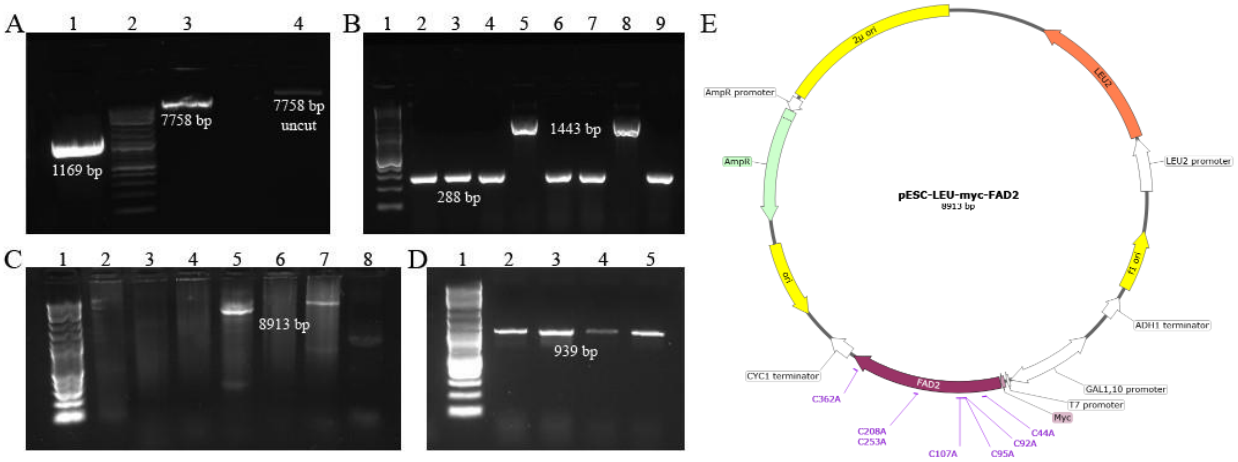

Figure 11. Representative ethidium bromide gel images of the process of generating the pESC-LEU-myc-FAD2 plasmids; each gel used NEB 1kb Plus DNA Ladder (New England BioLabs). A. Lane 1 shows successful PCR amplification of the WT FAD2 CDS with addition of XhoI restriction sites to both ends using pESC-LEU-myc-FAD2-LP and RP primers (Appendix A); Lane 2 shows the ladder; Lane 3 shows successful digestion of the pESC-LEU plasmid with XhoI; Lane 4 shows uncut pESC-LEU plasmid as a control. B. Lane 1 shows the ladder; Lanes 2-9 show E. coli *colony PCR products to verify pESC-LEU-myc-FAD2 transformation using Gal1Fw_V2 and Gal1Rv_V2 primers (Appendix A); only Lanes 5 and 8 indicate successful ligation and transformation. C. Lane 1 shows the ladder; Lanes 2-8 show SDM PCR products to generate Cys to Ala mutants C44A, C92A, C107A, C208A, C253A, and C362A, respectively, using corresponding forward and reverse primers (Appendix A); only Lanes 5 (C107A) and 7 (C253A) show successful products. D. Lane 1 shows the ladder; Lanes 2-5 show successful yeast colony PCR products to verify pESC-LEU-myc-FAD2-C107A transformation into yeast using Gal1Fw_V2 and Int_FAD2Rv primers (Appendix A). E. pESC-LEU-myc-FAD2 plasmid map shown via SnapGene.* Arabidopsis *FAD2 CDS is under a GAL1 promoter for galactose-induced expression, with C107A mutation location marked. Noteworthy features include ampicillin resistance, LEU2 for auxotrophic selection in yeast, and a myc tag.*

3.2 Protein-Protein Interaction Assays of FAD2

Since FAD2 has been previously reported to form a homodimer within *Arabidopsis* and *S. cerevisiae* (Lou et al. 2014), the involvement of the seven conserved cysteines in the PPI were evaluated on an individual basis through the mbSUS assay. To ensure that any changes in interactions were observed without potential hinderance from the split-ubiquitin halves fused to each protein, the following combinations were examined for each mutated protein for comparison with controls: mutant-Nub with mutant-Cub, mutant-Nub with wild-type-Cub, and

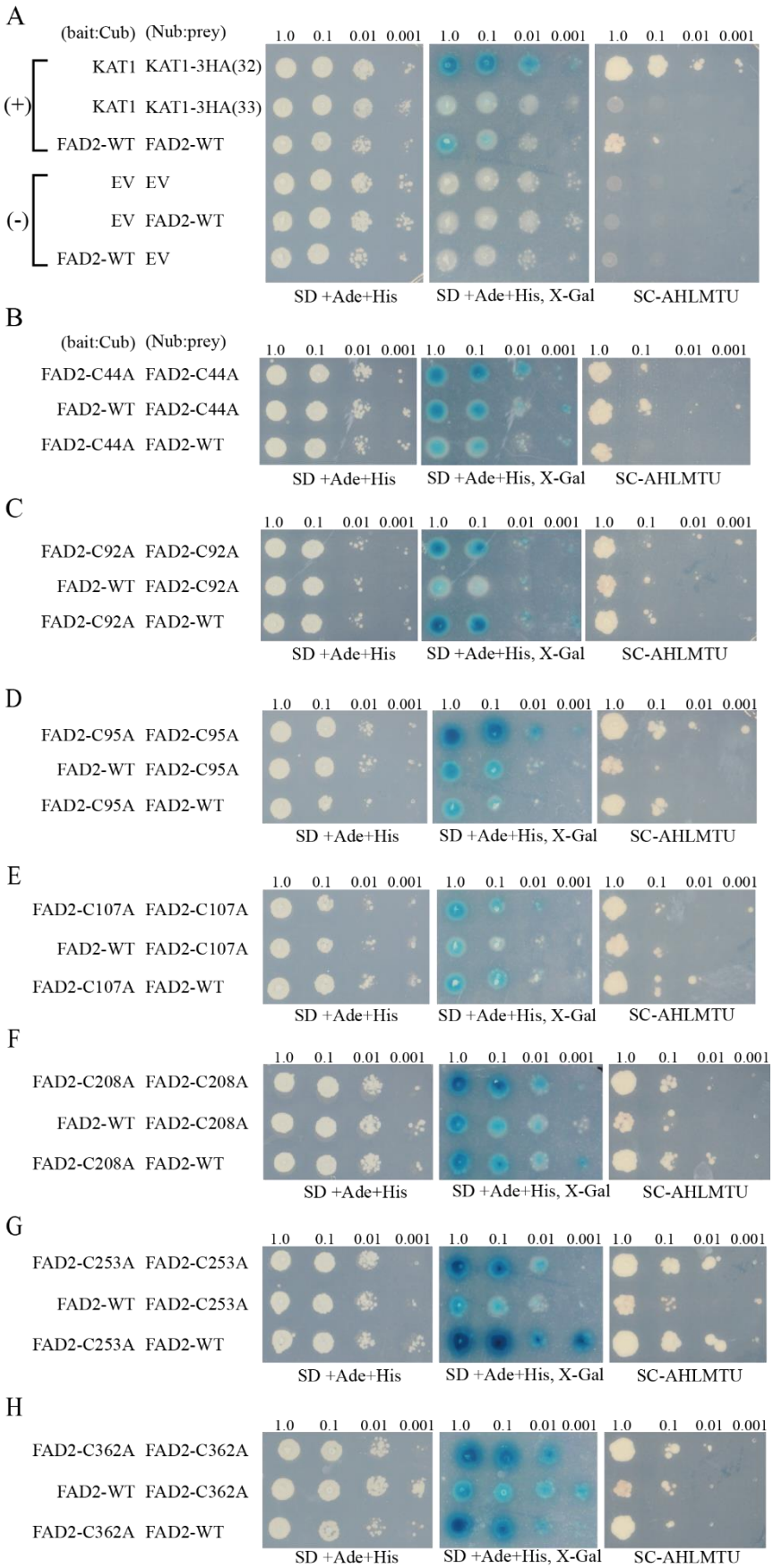
A
(bait:Cub) (Nub:prey)
KAT1 KAT1-3HA(32)
KAT1 KAT1-3HA(33)
FAD2-WT FAD2-WT
EV EV
EV FAD2-WT
FAD2-WT EV
(+)
(-)
1.0 0.1 0.01 0.001
SD +Ade+His
SD +Ade+His, X-Gal
SC-AHLMTU
B
(bait:Cub) (Nub:prey)
FAD2-C44A FAD2-C44A
FAD2-WT FAD2-C44A
FAD2-C44A FAD2-WT
C
FAD2-C92A FAD2-C92A
FAD2-WT FAD2-C92A
FAD2-C92A FAD2-WT
D
FAD2-C95A FAD2-C95A
FAD2-WT FAD2-C95A
FAD2-C95A FAD2-WT
E
FAD2-C107A FAD2-C107A
FAD2-WT FAD2-C107A
FAD2-C107A FAD2-WT
F
FAD2-C208A FAD2-C208A
FAD2-WT FAD2-C208A
FAD2-C208A FAD2-WT
G
FAD2-C253A FAD2-C253A
FAD2-WT FAD2-C253A
FAD2-C253A FAD2-WT
H
FAD2-C362A FAD2-C362A
FAD2-WT FAD2-C362A
FAD2-C362A FAD2-WT

Figure 12. PPIs detected between WT and the seven Cys to Ala mutated FAD2 proteins through mbSUS. A. Positive (+) and negative (-) controls display expected results- successful mating on SD+Ade+His; blue color change (+) indicating PPI and white colonies (-) indicating no PPI on SD+Ade+His, X-Gal; and growth (+) indicating PPI and no growth (-) indicating no PPI on SC-AHLMTU. B-H. The seven Cys to Ala mutated FAD2 proteins display successful mating (SD+Ade+His) and PPIs (SD+Ade+His, X-Gal and SC-AHLMTU) for each mating combination tested (n=3).

wild-type-Nub with mutant-Cub. Upon interaction of screened proteins, the Nub and Cub fusions are brought into close enough proximity to form semi-native ubiquitin which triggers ubiquitin specific proteases to cleave the protA-LexA-VP16 peptide from the Cub fusion, which then diffuses to the nucleus to activate lexA-regulated reporter genes. Transcription of the lacZ reporter gene which encodes the beta-galactosidase enzyme is detected through X-Gal overlay (where blue staining indicates an interaction, white indicates lack of interaction) and the Ade2 and His3 genes are detected through growth on auxotrophic selection plates. All of the cysteine-to-alanine mutated protein combinations screened through this assay displayed positive results (blue staining on SD+Ade+His plates overlayed with X-Gal which detects the transcription of the lacZ reporter gene and growth on auxotrophic selection media which demonstrates the transcription of the Ade2 and His3 reporter genes) indicating that the PPI was still able to occur between two FAD2 proteins despite the mutations (Fig. 12). These results, performed in triplicate after optimization (Appendix B), imply that on an individual basis, the seven conserved cysteines are not required to maintain PPIs in yeast. From this finding, there are three possible hypotheses for application to the structure of FAD2. First, without knowing how the FAD2 homodimer interacts or is formed due to minimal structural characterization of membrane-bound FADs, it is still possible that the cysteines are involved in the interactions, but the mutations to alanine are not enough to disrupt the intermolecular forces between the proteins, especially on an individual basis. This hypothesis, visually displayed through various interaction models generated via ClusPro displaying cysteines in interacting regions (Fig. 13A and B), has also been

observed in other experimentally assessed homodimers like chicken interleukin-2 where four cysteine residues on each protein had to be mutated to disrupt homodimerization, but single, double, or triple mutations had no effect (Deng et al. 2019). A second hypothesis is that the conserved cysteines are not on interacting regions of either protein, demonstrated through another ClusPro generated model (Fig. 13C), and therefore mutations to alanine would not affect interactions. The final hypothesis is that the conserved cysteines are not on the protein surface as suggested by the homology model, which could be supported by the fact that cysteines in proteins are often buried, especially those that are isolated (Marino & Gladyshev 2010).

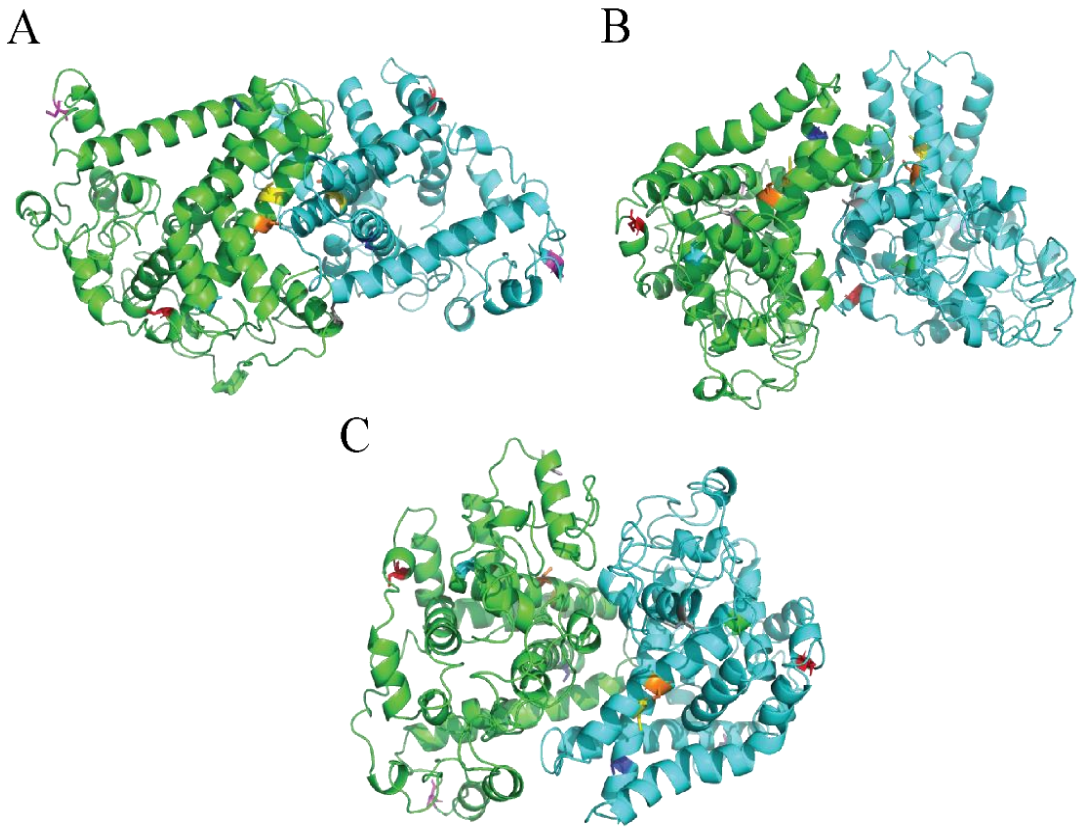

Figure 13. Potential FAD2 homodimer models generated via ClusPro with conserved cysteines labeled to demonstrate predicted involvement or lack of involvement in interactions, oriented to display interacting regions. A. Potential PPI displaying Cys92 (yellow), Cys95 (orange), and Cys362 (gray) in interacting regions of both proteins. B. Potential PPI displaying Cys95 (orange) and Cys362 (gray) in interacting regions of one protein. C. Potential PPI displaying none of the conserved cysteines in the interacting regions between proteins.

3.3 Protein Stability Analysis of FAD2

To investigate the roles of the conserved cysteines in the stability of FAD2, a cycloheximide chase assay was employed on *S. cerevisiae* cultures expressing pESC-LEU-myc-FAD2-WT or -C107A. The cycloheximide treatment was added to inhibit translation and thus further protein accumulation, and samples were collected for the wild-type protein at 0, 1, 2, 4, and 8 hours post-treatment, for the C107A protein at 0, 1, and 8 hours post-treatment, and at the same timepoints for both types of cultures treated with DMSO as a vehicle control. Western blot analysis using an anti-myc primary antibody probed for myc-FAD2 (~40 kDa), and stripping of those blots followed by re-probing with an anti-DPM1 primary antibody recognized endogenous DPM1 (35 kDa) which was used as a loading control. Analysis of FAD2-WT shows that the protein remains relatively stable up to eight hours post-treatment, with the calculated densitometric ratio of FAD2/DPM1 displaying a gradual decrease over time (Fig. 14A and B). These results are similar to those from previous studies of FAD2 from *Arabidopsis* and *Glycine max*, where the protein half-life was reported to be 4.74 hours (O'Quin et al. 2010; Tang et al. 2005). Comparison of FAD2-C107A to wild-type reveals a similar pattern of decrease over time, but results in lower levels of protein by the final timepoint indicating that the mutation causes a slight reduction in stability (Fig. 14C and D). This finding could explain the diminished FAD2 activity observed through preliminary lipid profile analysis (Fig. 8) and taken together would imply that Cys107 contributes necessary structural support for the protein. But as the decrease in stability is not as pronounced as the decrease in function, it is more likely that due to the proximity of Cys107 to the active site (Fig. 15), the mutation to alanine affects the structure of the active site, the ability of the conserved histidine boxes to coordinate iron, or the recognition

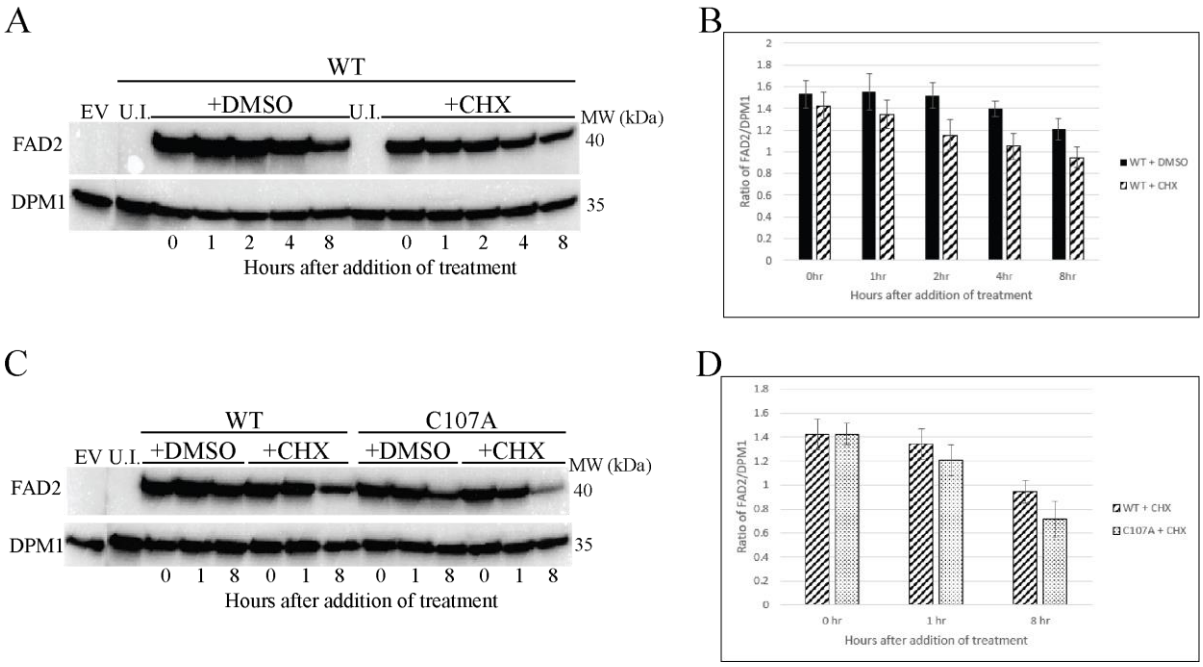

Figure 14. Western blot results and analysis of cycloheximide chase assay. A. Western blot results of assay performed on S. cerevisiae *expressing pESC-LEU-myc-FAD2-WT with samples taken at 0, 1, 2, 4, and 8 hours after treatment with DMSO (control) or CHX; top row probed for with anti-myc antibody, bottom with anti-DPM1 for a loading control. B. Densitometric analysis of FAD2/DPM1 ratio comparing FAD2-WT treated with DMSO or CHX across each timepoint. C. Western blot results of assay performed on* S. cerevisiae *expressing pESC-LEU-myc-FAD2-WT or -C107A with samples taken at 0, 1, and 8 hours after treatment with DMSO (control) or CHX; top row probed for with anti-myc antibody, bottom with anti-DPM1 for a loading control. D. Densitometric analysis of FAD2/DPM1 ratio comparing FAD2-WT and FAD2-C107A treated with CHX across each timepoint. Error bars represent ± S.E.M. of three experiments, n=3. EV= empty vector, U.I.= uninduced (both negative controls). Regions cropped from separate images of the same membrane that had been stripped. Unprocessed original scans of western blots shown in Appendix 3.*

and binding of the fatty acid substrates, thus indicating that Cys107 normally participates in one or more of those roles.

3.4 Functional Analysis of FAD2

To confirm the previously collected lipid profile analysis data to assess potentially modified FAD2 activity (the production of 16:2 or 18:2 fatty acids), samples were collected from cultures expressing pESC-LEU-myc-FAD2-WT and -C107A

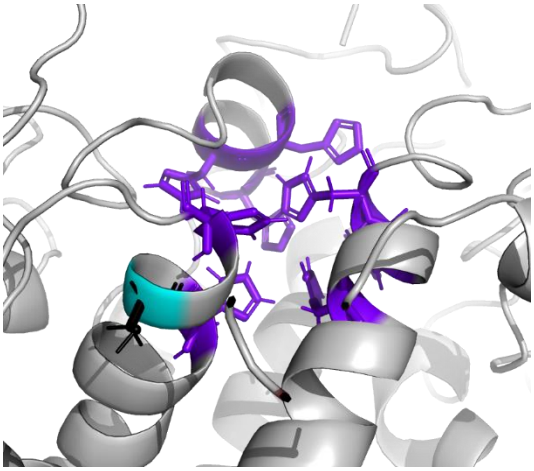

Figure 15. Cys107 (cyan) proximity to conserved histidine box (purple) active site of FAD2.

prior to the addition of treatments for the cycloheximide chase assay. As in Section 3.3, FAD2-C107A was the only mutated protein evaluated due to minimal success with site-directed mutagenesis, and use of the same plasmid for expression was desired to build upon protein stability data. Following lipid extraction, a gas chromatograph was used for compositional analysis to determine if Cys107 influences the biosynthetic activity of FAD2. Comparison of FAD2 product levels (16:2 and 18:2) between the wild-type and mutant samples shows no significant change (Fig. 16), a finding that is in direct contrast to previous data (Fig. 8). This disparity brings into question the validity of both sets of data, highlighting the need for further analysis to address potential causes. Possibilities include human error between experiments or variation in expression of FAD2 due to the change in plasmid used (pESC-HIS in preliminary, pESC-LEU

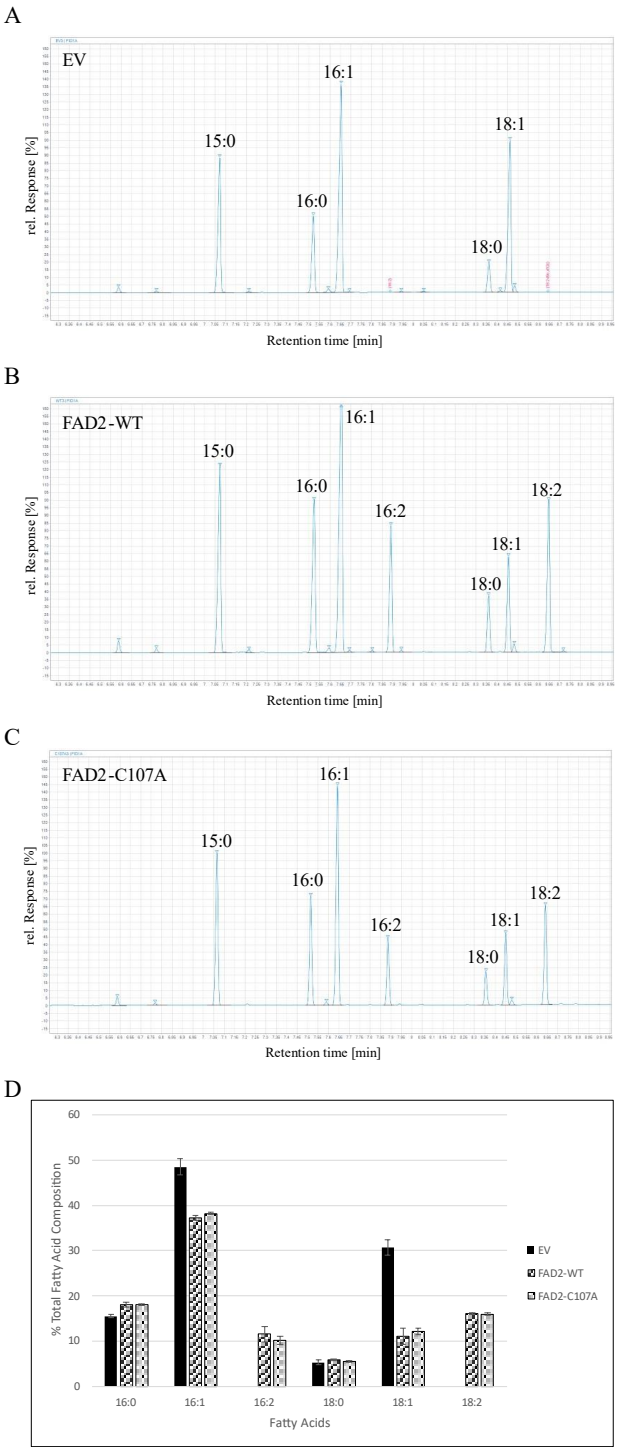

Figure 16. Lipid profile comparisons of S. cerevisiae *transformed with pESC-LEU-EV (A), pESC-LEU-FAD2-WT (B), and pESC-LEU-FAD2-C107A. A-C. Representative chromatograms for each respective sample type. D. Percent total fatty acid composition of each sample (n=2).*

current). Additionally, despite sequencing results indicating successful mutagenesis and protein stability data differing between the wild-type and mutant, there is a chance that SDM did not introduce the cysteine to alanine mutation. Finally, the myc or FLAG fusion tags could have altered protein activity, as an N-terminal myc tag has previously been observed to increase FAD2 activity (O'Quin et al. 2010), which could explain the increase in 16:2 and 18:2 fatty acids.

CHAPTER 4: FUTURE DIRECTIONS

To continue investigating the role of thiols in FAD2 and other desaturases, the remaining conserved cysteines (e.g. Cys44, 92, 95, 208, 253, and 362) should be evaluated for their potential roles in the stability of FAD2. This can be done through the previously described cycloheximide chase assay paired with Western blot analysis to round out the dataset. Lipid samples should also be collected from yeast cultures expressing each of these mutated proteins to confirm preliminary functionality results. The disparity between myc and FLAG tagged protein activity should be explored through comparison of lipid samples collected from yeast cultures expressing the respectively tagged proteins, an experiment which could potentially benefit from the addition of an untagged version of each protein being expressed. These untagged versions of FAD2-WT and each mutated FAD2 should provide an idea of what uninfluenced activity looks like, and therefore give further insight into the functional roles each conserved cysteine plays. An additional experiment that could expand upon the previously mentioned methods in yeast includes non-denaturing SDS-PAGE. I would expect cysteine-to-alanine mutations that are shown to decrease the stability of FAD2, like C107A, to also result in a decrease in dimer stability but not the ability to form the homodimer. Implementing a non-denaturing SDS-PAGE would bridge the concepts of homodimer interactions and stability if used in coordination with the cycloheximide chase assay because quantification of dimer formation and stability of each mutated protein would be possible.

As all previously described experiments are performed in yeast, the results should be verified in a plant system like *Arabidopsis* to ensure that any findings can be replicated in the protein's native environment. To test PPIs, bimolecular fluorescence complementation (BiFC) could be implemented as described (Waadt et al. 2014) using pSITE-nEYFP plasmids and

Agrobacterium to express each FAD2 protein in *Arabidopsis* leaves in comparison to FAD2-WT and KAT1 positive controls before interaction results are viewed with a confocal fluorescence microscope. Alternatively, co-immunoprecipitation (Co-IP) using antibodies specific to fused epitope tags followed by immunoblotting as outlined (Avila et al. 2015) could offer further insight into the homodimer interaction in a native environment and could also lead to assessing the heterodimer interaction with FAD3. To test stability, a similar cycloheximide chase assay could be applied in transgenic *Arabidopsis* seedlings as described (Gilkerson et al. 2016). These approaches, if results mirror those obtained in yeast, could help to refute potential claims of false positives from reporter systems (in PPI assays) and rule out the influence of any organism-specific factors (such as other proteins or cellular environment) on the gain or loss of stability of FAD2 and ability to interact.

Should the purification of FAD2 at experimental concentrations and in a native form be successful, as membrane-bound proteins pose a challenge in comparison to soluble proteins, *in vitro* methods that expand protein characterization could be employed. Pull-down assays would offer yet another avenue to explore PPIs between FAD2 and even FAD3 without the hindrance of tag-orientation within a membrane. Circular dichroism or hydrogen-deuterium exchange-mass spectrometry (HDX-MS) could experimentally determine elements of secondary or tertiary structure, folding properties, protein-ligand interactions, and allostery as well as the previously explored topics of stability and PPIs (Tsai et al. 2021; Greenfield 2006). These methods could provide support (or modifications) for the predicted structure of FAD2 as experimental verification is limited for membrane-bound proteins.

Apart from evaluating the roles of conserved cysteines in FAD2, other amino acids could similarly be assessed to determine involvement in stability, function, or interactions. Within all

FADs, seven prolines have also been found to be highly conserved. As proline is most commonly found in tight turns and is relatively non-reactive apart from roles in molecular recognition (Betts & Russell 2003), it could be an interesting subject of further investigation that could highlight a common structural feature of FADs. Deep mutational scanning (the use of next-generation sequencing, single amino acid mutagenesis, and functional assays (Starita & Fields 2015; Fowler & Fields 2014)) could shed light on other amino acids that play vital roles contributing to overall protein function, and therefore provide a more complete analysis of FAD2.

These findings and methods would not only contribute to the experimental determination of the structure of FAD2 from *Arabidopsis*, but also the many homologous FAD2 proteins that exist in plants ranging from eudicots, monocots, and lower plants (Cao et al. 2021). Past FAD2, the findings or at least the experimental setup to evaluate protein structure without common structural techniques could be employed on other uncharacterized FADs or membrane-bound proteins. Elucidating the structure of these enzymes will not only expand the field of knowledge in regard to FADs, but it will also present an opportunity to engineer these enzymes for increased stability (which could aid in plant growth and survival) or activity. These modifications may improve the field of metabolic engineering in relation to high-yield oil crops by improving production of PUFAs that are in high demand.

REFERENCES

Ahmad, A.; Ahsan, H. Lipid-Based Formulations in Cosmeceuticals and Biopharmaceuticals. *Biomedical Dermatology* **2020**, *4* (1), 12. https://doi.org/10.1186/s41702-020-00062-9.

Ambaye, T. G.; Vaccari, M.; Bonilla-Petriciolet, A.; Prasad, S.; van Hullebusch, E. D.; Rtimi, S. Emerging Technologies for Biofuel Production: A Critical Review on Recent Progress, Challenges and Perspectives. *Journal of Environmental Management* **2021**, *290*, 112627. https://doi.org/10.1016/j.jenvman.2021.112627.

Avila, J. R.; Lee, J. S.; Torii, K. U. Co-Immunoprecipitation of Membrane-Bound Receptors. *arbo.j* **2015**, *2015* (13). https://doi.org/10.1199/tab.0180.

Bassot, A.; Chen, J.; Simmen, T. Post-Translational Modification of Cysteines: A Key Determinant of Endoplasmic Reticulum-Mitochondria Contacts (MERCs). *Contact* **2021**, *4*, 25152564211001212. https://doi.org/10.1177/25152564211001213.

Ben Ayed, R.; Chirmade, T.; Hanana, M.; Khamassi, K.; Ercisli, S.; Choudhary, R.; Kadoo, N.; Karunakaran, R. Comparative Analysis and Structural Modeling of Elaeis Oleifera FAD2, a Fatty Acid Desaturase Involved in Unsaturated Fatty Acid Composition of American Oil Palm. *Biology* **2022**, *11* (4), 529. https://doi.org/10.3390/biology11040529.

Betts, M.J.; Russell, R.B. Amino acid properties and consequences of substitutions. In *Bioinformatics for Geneticists (First Edition)* **2003**; M.R. Barnes, I.C. Gray Eds, Wiley.

Biermann, U.; Bornscheuer, U. T.; Feussner, I.; Meier, M. A. R.; Metzger, J. O. Fatty Acids and Their Derivatives as Renewable Platform Molecules for the Chemical Industry. *Angewandte Chemie International Edition* **2021**, *60* (37), 20144–20165. https://doi.org/10.1002/anie.202100778.

Burns, A.; Olszowy, P.; Ciborowski, P. 2 - Biomolecules. In *Proteomic Profiling and Analytical Chemistry (Second Edition)* **2016**; Ciborowski, P., Silberring, J., Eds.; Elsevier: Boston; pp 7–24.

Cahoon, E. B.; Shanklin, J. Substrate-Dependent Mutant Complementation to Select Fatty Acid Desaturase Variants for Metabolic Engineering of Plant Seed Oils. *Proc Natl Acad Sci U S A* **2000**, *97* (22), 12350–12355.

Cao, S.; Zhang, J.; Cheng, H.; Aslam, M.; Lv, H.; Dong, W.; Hu, A.; Guo, M.; Liu, Q.; Qin, Y. Identification and Evolutionary Analysis of FAD2 Gene Family in Green Plants. *Tropical Plant Biol.* **2021**, *14* (3), 239–250. https://doi.org/10.1007/s12042-020-09276-x.

Chen, H.; Gu, Z.; Zhang, H.; Wang, M.; Chen, W.; Lowther, W. T.; Chen, Y. Q. Expression and Purification of Integral Membrane Fatty Acid Desaturases. *PLOS ONE* **2013**, *8* (3), e58139. https://doi.org/10.1371/journal.pone.0058139.

Chung, H. S.; Wang, S.-B.; Venkatraman, V.; Murray, C. I.; Van Eyk, J. E. Cysteine Oxidative Post-Translational Modifications: Emerging Regulation in the Cardiovascular System. *Circ Res* **2013**, *112* (2), 382–392. https://doi.org/10.1161/CIRCRESAHA.112.268680.

Deng, C.; Tan, H.; Zhou, H.; Wang, M.; Lü, Y.; Xu, J.; Zhang, H.; Han, L.; Ai, Y. Four Cysteine Residues Contribute to Homodimerization of Chicken Interleukin-2. *International Journal of Molecular Sciences* **2019**, *20* (22), 5744. https://doi.org/10.3390/ijms20225744.

Dyer, J. M.; Mullen, R. T. Immunocytological Localization of Two Plant Fatty Acid Desaturases in the Endoplasmic Reticulum. *FEBS Letters* **2001**, *494* (1), 44–47. https://doi.org/10.1016/S0014-5793(01)02315-8.

Fomenko, D. E.; Gladyshev, V. N. CxxS: Fold-Independent Redox Motif Revealed by Genome-Wide Searches for Thiol/Disulfide Oxidoreductase Function. *Protein Sci* **2002**, *11* (10), 2285–2296.

Fowler, D. M.; Fields, S. Deep Mutational Scanning: A New Style of Protein Science. *Nat Methods* **2014**, *11* (8), 801–807. https://doi.org/10.1038/nmeth.3027.

Fra, A.; Yoboue, E. D.; Sitia, R. Cysteines as Redox Molecular Switches and Targets of Disease. *Frontiers in Molecular Neuroscience* **2017**, *10*.

Gilkerson, J.; Tam, R.; Zhang, A.; Dreher, K.; Callis, J. Cycloheximide Assays to Measure Protein Degradation in Vivo in Plants. *Bio-protocol* **2016**, *6* (17), e1919–e1919.

Gladyshev, V. N.; Kryukov, G. V.; Fomenko, D. E.; Hatfield, D. L. Identification of Trace Element-Containing Proteins in Genomic Databases. *Annu Rev Nutr* **2004**, *24*, 579–596. https://doi.org/10.1146/annurev.nutr.24.012003.132241.

Greenfield, N. J. Using Circular Dichroism Spectra to Estimate Protein Secondary Structure. *Nat Protoc* **2006**, *1* (6), 2876–2890. https://doi.org/10.1038/nprot.2006.202.

Halim, N. F. A. A.; Ali, M. S. M.; Leow, A. T. C.; Rahman, R. N. Z. R. A. Membrane Fatty Acid Desaturase: Biosynthesis, Mechanism, and Architecture. *Appl Microbiol Biotechnol* **2022**, *106* (18), 5957–5972. https://doi.org/10.1007/s00253-022-12142-3.

Horn, P. J.; Smith, M. D.; Clark, T. R.; Froehlich, J. E.; Benning, C. PEROXIREDOXIN Q Stimulates the Activity of the Chloroplast 16:1Δ3trans FATTY ACID DESATURASE4. *The Plant Journal* **2020**, *102* (4), 718–729. https://doi.org/10.1111/tpj.14657.

Lee, J. M.; Lee, H.; Kang, S.; Park, W. J. Fatty Acid Desaturases, Polyunsaturated Fatty Acid Regulation, and Biotechnological Advances. *Nutrients* **2016**, *8* (1), 23. https://doi.org/10.3390/nu8010023.

Li, D.; Moorman, R.; Vanhercke, T.; Petrie, J.; Singh, S.; Jackson, C. J. Classification and Substrate Head-Group Specificity of Membrane Fatty Acid Desaturases. *Computational*

and Structural Biotechnology Journal **2016**, *14*, 341–349. https://doi.org/10.1016/j.csbj.2016.08.003.

Lou, Y.; Schwender, J.; Shanklin, J. FAD2 and FAD3 Desaturases Form Heterodimers That Facilitate Metabolic Channeling in Vivo*. *Journal of Biological Chemistry* **2014**, *289* (26), 17996–18007. https://doi.org/10.1074/jbc.M114.572883.

Lou, Y.; Shanklin, J. Evidence That the Yeast Desaturase Ole1p Exists as a Dimer in Vivo. *J Biol Chem* **2010**, *285* (25), 19384–19390. https://doi.org/10.1074/jbc.M110.125377.

Marino, S. M.; Gladyshev, V. N. Analysis and Functional Prediction of Reactive Cysteine Residues. *J Biol Chem* **2012**, *287* (7), 4419–4425. https://doi.org/10.1074/jbc.R111.275578.

Marino, S. M.; Gladyshev, V. N. Cysteine Function Governs Its Conservation and Degeneration and Restricts Its Utilization on Protein Surfaces. *J Mol Biol* **2010**, *404* (5), 902–916. https://doi.org/10.1016/j.jmb.2010.09.027.

Marino, S. M.; Salinas, G.; Gladyshev, V. N. Chapter 3 - Computational Functional Analysis of Cysteine Residues in Proteins. In *Redox Chemistry and Biology of Thiols*; Alvarez, B., Comini, M. A., Salinas, G., Trujillo, M., Eds.; Academic Press, 2022; pp 59–80. https://doi.org/10.1016/B978-0-323-90219-9.00015-7.

Muro, E.; Atilla-Gokcumen, G. E.; Eggert, U. S. Lipids in Cell Biology: How Can We Understand Them Better? *Mol Biol Cell* **2014**, *25* (12), 1819–1823. https://doi.org/10.1091/mbc.E13-09-0516.

Murphy, D. J. Plant Storage Lipids. In *eLS*; John Wiley & Sons, Ltd, **2016**; pp 1–7. https://doi.org/10.1002/9780470015902.a0001918.pub3.

Nachtschatt, M.; Okada, S.; Speight, R. Integral Membrane Fatty Acid Desaturases: A Review of Biochemical, Structural, and Biotechnological Advances. *European Journal of Lipid Science and Technology* **2020**, *122* (12), 2000181. https://doi.org/10.1002/ejlt.202000181.

Nguyen, V. C.; Nakamura, Y.; Kanehara, K. Membrane Lipid Polyunsaturation Mediated by FATTY ACID DESATURASE 2 (FAD2) Is Involved in Endoplasmic Reticulum Stress Tolerance in Arabidopsis Thaliana. *The Plant Journal* **2019**, *99* (3), 478–493. https://doi.org/10.1111/tpj.14338.

O'Quin, J. B.; Bourassa, L.; Zhang, D.; Shockey, J. M.; Gidda, S. K.; Fosnot, S.; Chapman, K. D.; Mullen, R. T.; Dyer, J. M. Temperature-Sensitive Post-Translational Regulation of Plant Omega-3 Fatty-Acid Desaturases Is Mediated by the Endoplasmic Reticulum-Associated Degradation Pathway. *J Biol Chem* **2010**, *285* (28), 21781–21796. https://doi.org/10.1074/jbc.M110.135236.

Obrdlik, P. Manual for the use of mating-based split ubiquitin system "mbSUS". *Carnegie Science* **2004.**

Ohlrogge, J.; Browse, J. Lipid Biosynthesis. *Plant Cell* **1995**, *7* (7), 957–970.

Shanklin, J.; Cahoon, E. B. Desaturation and Related Modifications of Fatty Acids. *Annual Review of Plant Physiology and Plant Molecular Biology* **1998**, *49* (1), 611–641. https://doi.org/10.1146/annurev.arplant.49.1.611.

Simopoulos, A. P. An Increase in the Omega-6/Omega-3 Fatty Acid Ratio Increases the Risk for Obesity. *Nutrients* **2016**, *8* (3), 128. https://doi.org/10.3390/nu8030128.

Simopoulos, A. P. The Omega-6/Omega-3 Fatty Acid Ratio: Health Implications. *OCL* **2010**, *17* (5), 267–275. https://doi.org/10.1051/ocl.2010.0325.

Sliwoski, G.; Kothiwale, S.; Meiler, J.; Lowe, E. W. Computational Methods in Drug Discovery. *Pharmacol Rev* **2014**, *66* (1), 334–395. https://doi.org/10.1124/pr.112.007336.

Starita, L. M.; Fields, S. Deep Mutational Scanning: A Highly Parallel Method to Measure the Effects of Mutation on Protein Function. *Cold Spring Harb Protoc* **2015**, *2015* (8), pdb.top077503. https://doi.org/10.1101/pdb.top077503.

Sun, M.; Wang, Y.; Zhang, Q.; Xia, Y.; Ge, W.; Guo, D. Prediction of Reversible Disulfide Based on Features from Local Structural Signatures. *BMC Genomics* **2017**, *18* (1), 279. https://doi.org/10.1186/s12864-017-3668-8.

Tang, G.-Q.; Novitzky, W. P.; Carol Griffin, H.; Huber, S. C.; Dewey, R. E. Oleate Desaturase Enzymes of Soybean: Evidence of Regulation through Differential Stability and Phosphorylation. *The Plant Journal* **2005**, *44* (3), 433–446. https://doi.org/10.1111/j.1365-313X.2005.02535.x.

Tsai, W.-C.; Aleem, A. M.; Whittington, C.; Cortopassi, W. A.; Kalyanaraman, C.; Baroz, A.; Iavarone, A. T.; Skrzypczak-Jankun, E.; Jacobson, M. P.; Offenbacher, A. R.; Holman, T. Mutagenesis, Hydrogen–Deuterium Exchange, and Molecular Docking Investigations Establish the Dimeric Interface of Human Platelet-Type 12-Lipoxygenase. *Biochemistry* **2021**, *60* (10), 802–812. https://doi.org/10.1021/acs.biochem.1c00053.

Waadt, R.; Schlücking, K.; Schroeder, J. I.; Kudla, J. Protein Fragment Bimolecular Fluorescence Complementation Analyses for the in Vivo Study of Protein-Protein Interactions and Cellular Protein Complex Localizations. *Methods Mol Biol* **2014**, *1062*, 629–658. https://doi.org/10.1007/978-1-62703-580-4_33.

Whelan, J.; Fritsche, K. Linoleic Acid. *Adv Nutr* **2013**, *4* (3), 311–312. https://doi.org/10.3945/an.113.003772.

Zhang, J.; Liu, H.; Sun, J.; Li, B.; Zhu, Q.; Chen, S.; Zhang, H. Arabidopsis Fatty Acid Desaturase FAD2 Is Required for Salt Tolerance during Seed Germination and Early Seedling Growth. *PLOS ONE* **2012**, *7* (1), e30355. https://doi.org/10.1371/journal.pone.0030355.

APPENDIX A: LIST OF PRIMERS

Primer ID	Sequence	Purpose
M13/pUC Reverse	AGCGGATAACAATTTCACACAGG	mbSUS Sequencing/ Genotyping
M13 Reverse	CAGGAAACAGCTATGAC	mbSUS Sequencing/ Genotyping
M13 Forward	TGTAAAACGACGGCCAGT	mbSUS Sequencing/ Genotyping
M13/pUC Forward	CCCAGTCACGACGTTGTAAAACG	mbSUS Sequencing/ Genotyping
Kan-F	TTCCTTTTAAAATCTTGCTAGGATACA	mbSUS Sequencing/ Genotyping
Kan-F2	TTGTTTTCAAGAACTTGTCATTTG	mbSUS Sequencing/ Genotyping
Kan-R	ATCGCGAGCCCATTTATACC	mbSUS Sequencing/ Genotyping
LexA F	ACGCAAAGGCGTTATTGAAA	mbSUS Sequencing/ Genotyping
KAT1-Fw	GGATTGGAGCTGTGTATCCAA	mbSUS Sequencing/ Genotyping

KAT1-Rv	TTCTCAAGCCTTGCAAATAGC	mbSUS Sequencing/ Genotyping
mbSUSB1Fw-FAD2	ACAAGTTTGTACAAAAAAGCAGGCTCTCCAACCACCATGGGTGCAGGTGGAAGA	mbSUS Cloning
mbSUSB2Rv-FAD2	TCCGCCACCACCAACCACTTTGTACAAGAAAGCTGGGTATAACTTATTGTTGTACCAGTA	mbSUS Cloning
attB1Fw	ACAAGTTTGTACAAAAAAGCAGGCT	mbSUS Sequencing/ Genotyping
attB2Fw	ACCCAGCTTTCTTGTACAAAGTGGT	mbSUS Sequencing/ Genotyping
attB1RvComp	AGCCTGCTTTTTTGTACAAACTTGT	mbSUS Sequencing/ Genotyping
attB2RvComp	ACCACTTTGTACAAGAAAGCTGGGT	mbSUS Sequencing/ Genotyping
AtFAD2Cys44Ala_F2	GCCGCATGCTTTCAAACGCTCAATC	SDM
AtFAD2Cys44Ala_R2	GGGATTGCTTTCTTCAGATCTCCC	SDM
AtFAD2Cys44Ala_R3	ATTGCTTTCTTCAGATCTCCCACC	SDM
FAD2CYS44_DELFW	TTCTCGGTGGGAGATCTGAAGAAAG	SDM
FAD2CYS44_DELRV	AGGCGGTTTCTCGCACGG	SDM

FAD2CYS44_coFW	CACCTCACGCTTTCAAACGCTCAATCCCTC	SDM
FAD2CYS44_coRv	GAATAGCCTTTTTCAGATCTCCCACCGAG	SDM
AtFAD2Cys92Ala_F	CTATTGGGCCGCTCAAGGCTGTGTCC	SDM
AtFAD2Cys92Ala_R	AGTGGCCAAGCCAAGTA	SDM
AtFAD2Cys95Ala_F	CTGTCAAGGCGCTGTCCTAACTGGTATCTGG	SDM
AtFAD2Cys95Ala_R	GCCCAATAGAGTGGCCAA	SDM
AtFAD2Cys107Ala_F	AGCCCACGAAGCTGGTCACCACG	SDM
AtFAD2Cys107Ala_R	ATGACCCAGATACCAGTTAG	SDM
AtFAD2Cys208Ala_F	CGGGTTCGCTGCTCATTTCTTCCCC	SDM
AtFAD2Cys208Ala_R	TCATACGGTCTGCCAGAG	SDM
AtFAD2Cys253Ala_F	CTCGATGATCGCTCTCTACGGAGTACCGCTTC	SDM
AtFAD2Cys253Ala_R	GCCATCCCTTGTGCAGCA	SDM
AtFAD2Cys362Ala_F	GGCAAAGGAGGCTATCTATGTAGAACCG	SDM
AtFAD2Cys362Ala_R	TCCCTATACATCGCTACATAC	SDM
GAL1 Fw	ATTTTCGGTTTGTATTACTTC	Sequencing/ Genotyping

GAL1 Rv	GTTCTTAATACTAACATAACT	Sequencing/ Genotyping
Gal1Fw_V2	TCAACATTTTCGGTTTGTATTACTTC	Sequencing/ Genotyping
Gal1Rv_V2	AAATAGGGACCTAGACTTCAGGTTG	Sequencing/ Genotyping
myc-FAD2_Fw	GCCGTCGACAAAAATGGAACAGAAGTTGATTTCCGAAGAAGACCTCGGTGCAGGTGGAAGAATGC	Cloning
myc-FAD2_Rv	CTTACTCGAGTCATGCTAACTTATTGTTGTACCAGTACACAC	Cloning
pESC-LEU-myc-FAD2-LP	AGACCTCGAGGGTGCAGGTGGAAGAATGC	Cloning
pESC-LEU-myc-FAD2-RP	CTTACTCGAGTGCTAACTTATTGTTGTACCAGTACACAC	Cloning
Int_FAD2Fw	TCCTTCCTCCTCGTCCCTTA	Internal sequencing
Int_FAD2Rv	CCGTAGAGGCAGATCATCGA	Internal sequencing

APPENDIX B: mbSUS PROTOCOL OPTIMIZATION

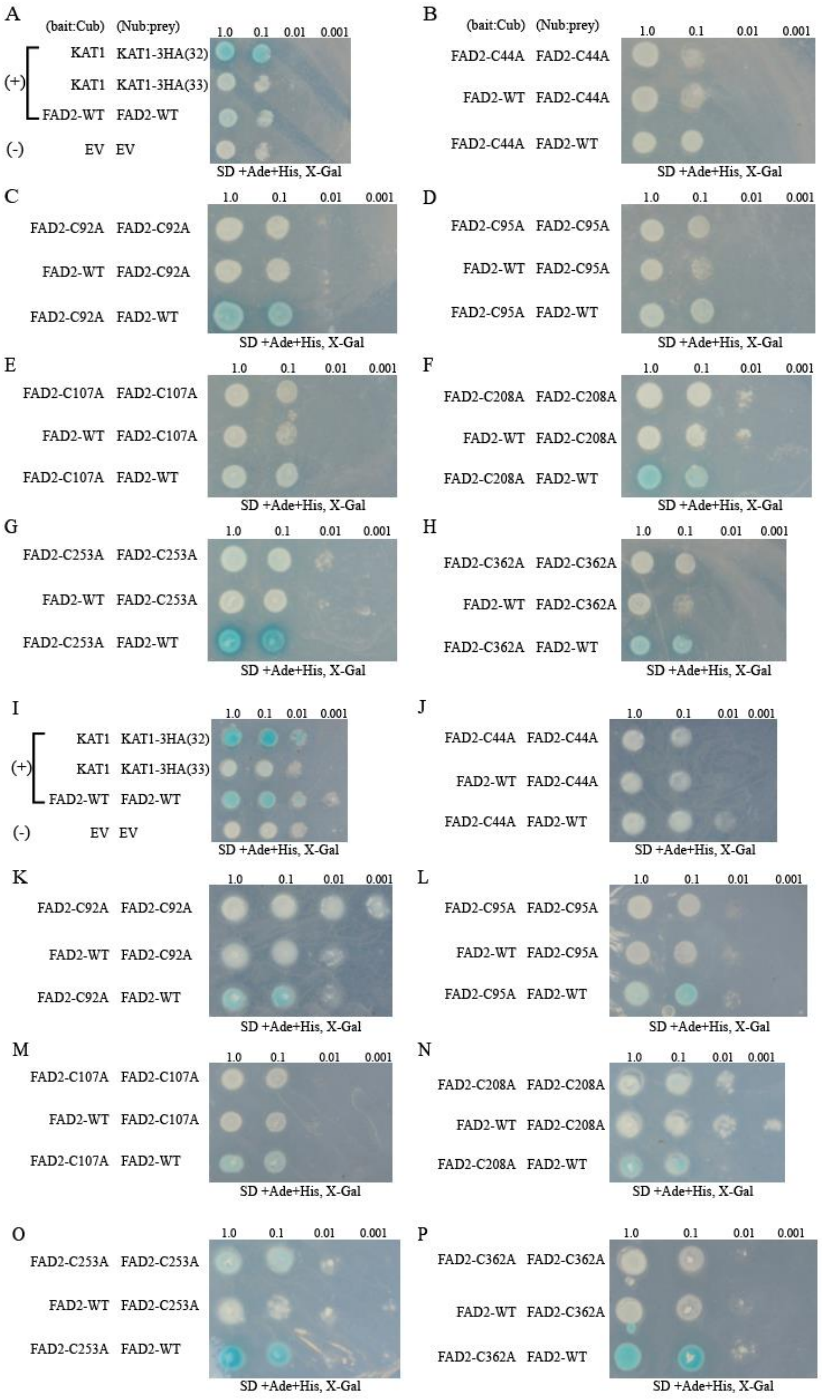

Figure 17. Optimization of mbSUS protocol to detect PPIs between WT and the seven Cys to Ala mutated FAD2 proteins. A-H. Initial PPI results showing few and weak positive results on SD+Ade+HIS, X-Gal using the Nub construct pNXgate33-3HA (low copy). I-P. Subsequent PPI results showing stronger positive results on SD+Ade+His, X-Gal using the Nub construct pNXgate33-3HA (low copy) and chloroform to permeabilize cells to the X-Gal substrate.

APPENDIX C: UNPROCESSED WESTERN BLOTS

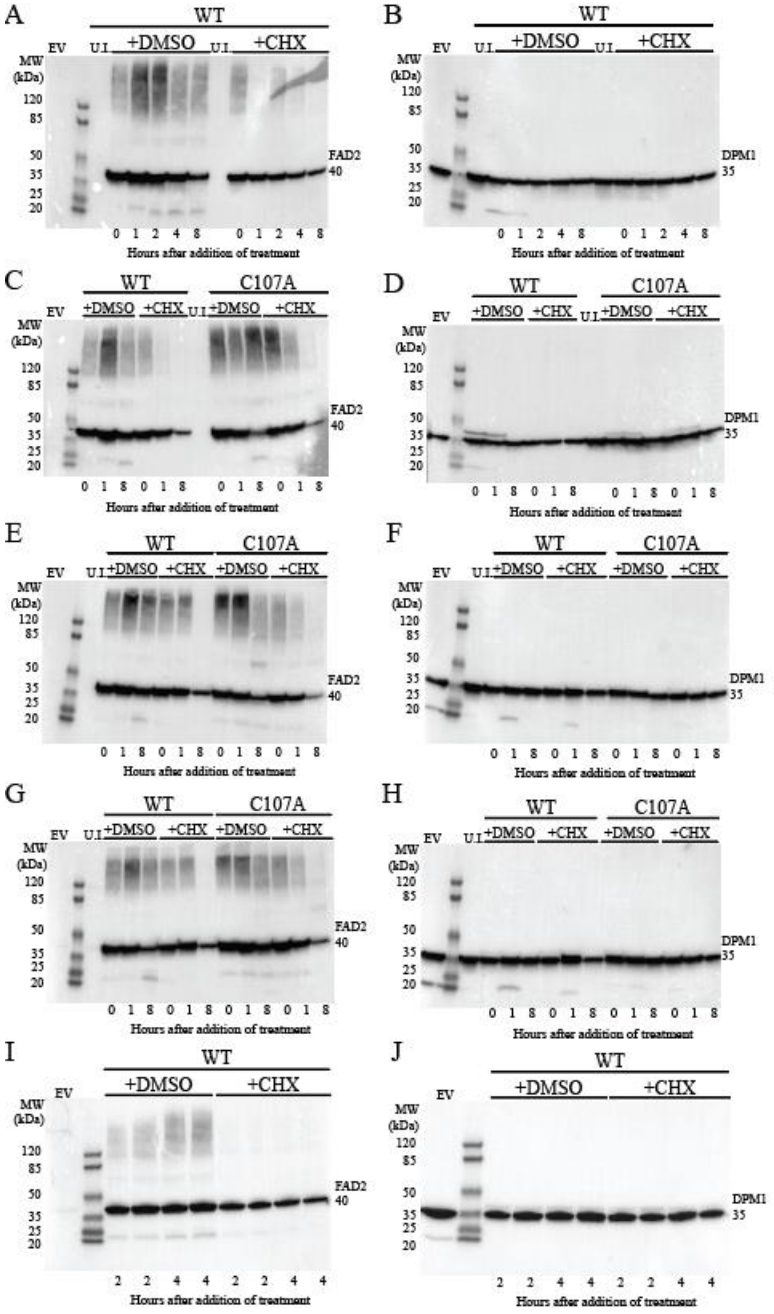

Figure 18. Full Western blot results to generate three biological replicates of FAD2-WT and C107A proteins from cycloheximide chase assays. A, C, E, G, I. Blots for FAD2 protein using anti-myc primary antibody. B, D, F, H, J. Blots for DPM1 endogenous loading control protein using anti-DPM1 primary antibody generated by stripping each blot to the left, respectively, and reprobing.